Research Square

Preprints are preliminary reports that have not undergone peer review.
They should not be considered conclusive, used to inform clinical practice,
or referenced by the media as validated information.

Mitochondrial capacity limits neuronal energetic feasibility under chronic behavioural stress associated with AI-intensive environments: a neuron–astrocyte genome-scale model of human grey matter

Shangwe Leonard Kigoda
The Nelson Mandela African Institution of Science and Technology (NM-AIST)
Christina Charles
BioNutra Company Limited
Musa Chacha
The Nelson Mandela African Institution of Science and Technology (NM-AIST)
Jofrey Raymond
jofrey.raymond@nm-aist.ac.tz
The Nelson Mandela African Institution of Science and Technology (NM-AIST)

Research Article

Keywords: Brain energy metabolism, Neuron–astrocyte coupling, Glutamate–glutamine cycle, Sleep loss, Genome-scale metabolic model, Mitochondrial capacity

Posted Date: November 16th, 2026

DOI: https://doi.org/10.21203/rs.3.rs-11551364/v1

License: This work is licensed under a Creative Commons Attribution 4.0 International License.
Read Full License

Additional Declarations: No competing interests reported.

Mitochondrial capacity limits neuronal energetic feasibility under chronic behavioural stress associated with AI-intensive environments: a neuron–astrocyte genome-scale model of human grey matter

Shangwe Leonard Kigoda[1], Christina Charles[2], Musa Chacha[1], Jofrey Raymond[1,2*]

[1] School of Life Sciences and Bioengineering, The Nelson Mandela African Institution of Science and Technology (NM-AIST), P.O. Box 447, Arusha, Tanzania

[2] BioNutra Company Limited, Arusha, Tanzania

* Corresponding author: Jofrey Raymond, jofrey.raymond@nm-aist.ac.tz; ORCID 0000-0002-3500-2183

Email addresses: Shangwe Leonard Kigoda kigodas@nm-aist.ac.tz; Christina Charles ceo@bionutraplatform.com; Musa Chacha musa.chacha@nm-aist.ac.tz; Jofrey Raymond jofrey.raymond@nm-aist.ac.tz

Article type: Original Research

Abstract

Sustained cognitive engagement, short and mistimed sleep, chronic stress and reduced recovery co-occur in AI-intensive environments, yet how this profile acts on brain energy metabolism is unknown. We built a neuron–astrocyte genome-scale model of human grey matter from Human-GEM v2.1.1, contextualised each cell with human single-nucleus expression, made transport, sodium-pumping and glutathione-recycling costs explicit, and calibrated one parameter to measured cerebral glucose use. Without further fitting the model reproduced the astrocytic share of oxidative metabolism measured by ^{13}C spectroscopy (15.7% vs 14%), both the oxidative and the glycolytic regimes of human brain activation, and an independent reconstruction; deletion of genes causing inherited brain-energy disorders compromised its energetic margin far more often than deletion of other genes (odds ratio 79, $p = 6 \times 10^{-20}$). Translating the five stressors into constraints, sleep loss and cognitive load each exhausted the margin within the protocol range, at a 25% loss of mitochondrial capacity and a 39% rise in signalling demand, whereas circadian misalignment, chronic stress and reduced recovery acted on arms with reserve. Combined, the stressors exhausted the margin at 0.72 times the moderate profile; across 400 parameter draws demand was met in 99.2% at low and 28.5% at moderate exposure. Substrate oxidation, not substrate supply, set the margin: restoring sleep or reducing load restored it, whereas ketone bodies, lactate or fibre-derived acetate helped only when glucose delivery itself was limiting. Results held across thresholds, releases, solvers and enzyme-capacity limits, and the thresholds are testable with ^{31}P and ^{13}C spectroscopy.

Keywords: Brain energy metabolism; Neuron–astrocyte coupling; Glutamate–glutamine cycle; Sleep loss; Genome-scale metabolic model; Mitochondrial capacity

Introduction

The adult human brain accounts for about 2% of body mass yet consumes roughly a fifth of resting energy (Aiello and Wheeler 1995; Herculano-Houzel 2011), and it does so with almost no reserve. Neurons hold negligible glycogen, and astrocytic glycogen—about 3.5 μmol g^{-1} in the human brain, roughly ten minutes of resting glucose use (Öz et al. 2007)—sustains function for tens of minutes when supply fails (Brown and Ransom 2007), and most of the ATP that grey matter produces is spent restoring the ion gradients that action potentials and synaptic transmission dissipate (Attwell and Laughlin 2001; Harris et al. 2012). Because this work is continuous, cerebral function depends on a narrow match between the demand set by signalling and the capacity of glucose delivery, mitochondrial oxidation and antioxidant recycling to meet it (Dienel 2019; Rae et al. 2024). Disturbances in each of these supply arms precede cognitive decline by years: regional glucose hypometabolism, impaired oxidative phosphorylation and oxidative stress are among the earliest measurable changes in the ageing and neurodegenerating brain (Halliwell 2006; Cunnane et al. 2020).

Energy supply in grey matter is a property of two cooperating cell types rather than of neurons alone. Glutamate released at excitatory synapses is cleared mainly by astrocytic transporters that carry three Na^+ ions with each glutamate (Zerangue and Kavanaugh 1996; Levy et al. 1998; Danbolt 2001); astrocytes convert it to glutamine through glutamine synthetase, an astrocyte-restricted enzyme (Norenberg and Martinez-Hernandez 1979), and return it to neurons, which hydrolyse it to refill the transmitter pool. ^{13}C magnetic resonance spectroscopy has measured this glutamate–glutamine cycle at about 0.3 μmol g^{-1} min^{-1} in the human cortex (Shen et al. 1999), and in the rat the cycle rises almost one-for-one with neuronal glucose oxidation (Sibson et al. 1998), while astrocytes contribute about one-seventh of cerebral oxidative metabolism in humans (Lebon et al. 2002), with estimates from other approaches of up to about 30% (Hertz et al. 2007). Whether astrocytes also export lactate to

fuel neurons remains disputed (Pellerin and Magistretti 1994; Mächler et al. 2016; Díaz-García et al. 2017; Yellen 2018). Any account of how chronic behavioural pressure erodes brain energetics therefore has to represent both cells, the transport between them, and the costs of the cycle that links them (Bélanger et al. 2011; Magistretti and Allaman 2015).

The behavioural pressures in question have changed in kind. Work and study in AI-intensive environments—conversational agents, recommendation systems and algorithmically sequenced tasks—raise the density and duration of cognitive engagement, encourage task switching and late-evening screen use—our premise—while evening use of light-emitting screens is known to delay sleep and circadian timing (Chang et al. 2015; Hale and Guan 2015) and digital tools to encourage cognitive offloading (Risko and Gilbert 2016; Gerlich 2025). None of these stressors is new on its own. Sustained cognitive work raises local cerebral energy use (Lin et al. 2010; Jamadar et al. 2025); sleep loss reduces cerebral glucose use, at least regionally, and in animals depletes energy stores that recover during sleep (Wu et al. 1991; Benington and Heller 1995; Thomas et al. 2000; Kong et al. 2002; Dworak et al. 2010); circadian misalignment and chronic psychosocial stress impair glucose handling and mitochondrial function (McEwen 1998; Spiegel et al. 1999; Scheer FAJL et al. 2009; Picard and McEwen 2018); and sleep loss raises oxidative load (Vaccaro et al. 2020; Haynes et al. 2024). What such environments add is their co-occurrence and persistence. Studies of AI-related fatigue and dependence measure attention, performance or self-report, which are late, functional readouts; none asks how the combined load reshapes the biochemical limits within which neurons and astrocytes can meet their demand.

Genome-scale metabolic models can ask that question directly. They represent the stoichiometry of thousands of reactions and treat a physiological state as feasible when some flux distribution satisfies every mass balance, capacity limit and demand at once (Ebrahim et al. 2013; Robinson et al. 2020). Earlier neuron–astrocyte reconstructions established that

constraint-based models reproduce the main features of brain energy metabolism (Çakır et al. 2007; Lewis et al. 2010b; Sertbaş et al. 2014), but they were built on small or generic networks, were not contextualised with human single-cell expression, and did not examine chronic behavioural stressors. Here we built a two-cell model of human grey matter from Human-GEM v2.1.1, contextualised each cell with single-nucleus expression from the Human Protein Atlas (Karlsson et al. 2021; Siletti et al. 2023), enforced the transport, ion and redox costs that couple the two cells, and calibrated a single parameter to the measured cerebral glucose use. We then translated five chronic behavioural stressors into explicit constraints, quantified how far each and their combination erode the energetic margin of the unit, located the thresholds at which neuronal demand can no longer be met, and tested the model against independent human measurements and against the genetics of inherited brain-energy disorders.

Materials and Methods

Study design and computational environment

This is a computational study that uses only public reconstructions and public, de-identified expression data. The analysis followed five stages: construction and contextualisation of the two-cell model; physiological calibration and validation of the resting state; translation of behavioural stressors into constraints; constraint-based feasibility, flexibility, sensitivity and threshold analyses; and robustness tests across thresholds, reconstructions, releases and solvers. All analyses were run on a workstation with an Intel Core i9-9880H processor (2.3 GHz, 8 cores, 16 threads) and 32 GB RAM under macOS 13.0, using Python 3.9.6, COBRApy 0.31.1 (Ebrahim et al. 2013), optlang 1.9.1 (Jensen et al. 2017), the GNU Linear Programming Kit through swiglpk 5.0.13, HiGHS 1.15.1 (highspy) for solver replication (Huangfu and Hall 2018), SALib 1.5.2 (Herman and Usher 2017), NumPy 2.0.2, pandas 2.3.3,

SciPy 1.13.1 and Matplotlib 3.9.4. Fluxes are expressed in μmol per gram of wet tissue per minute (μmol g^{-1} min^{-1}), the unit in which human cerebral metabolic rates are reported. All analyses were performed on the in-house BioNutra metabolic-modelling facility. A generative-AI tool assisted with grammar and with drafting the authors' text into academic language, and with preparing and checking analysis and figure-plotting scripts under the authors' direction. Every numerical result was produced by the stated open-source software (COBRApy, SALib) and can be regenerated from the deposited code. The authors checked all content and take full responsibility for it.

Reconstruction and expression data

The reconstruction was Human-GEM v2.1.1 (SysBioChalmers, released October 2026; 12,748 reactions, 8,374 metabolites, 2,870 genes; SBML file SHA-256 dc0efd8009a8b680bde7040440f2e3592027dd118833445092ebd8d7bc425ddf) (Robinson et al. 2020). Cell-type expression was taken from the Human Protein Atlas single-cell type table (normalised transcripts per million, nCPM), which integrates single-nucleus sequencing of the human brain (Uhlén et al. 2015; Karlsson et al. 2021; Siletti et al. 2023). The neuronal profile was the mean of brain excitatory and inhibitory neurons; the astrocytic profile was the astrocyte cluster. Of the 2,870 model genes, 2,865 were present in the table. Regional bulk expression (normalised TPM for eight brain regions) was taken from the Human Protein Atlas brain-region table (Sjöstedt et al. 2020). All files were downloaded in October 2026.

Contextualisation and curation

Reaction expression was computed from gene–protein–reaction rules (minimum over subunits joined by AND, maximum over isozymes joined by OR). Each cell type was contextualised with GIMME (Becker and Palsson 2008). Under a generous medium, the maximal ATP hydrolysis flux (Human-GEM MAR03964) was computed with the cell's defining task

imposed—release of 0.32 μmol g^{-1} min^{-1} glutamate for the neuron, release of the same amount of glutamine for the astrocyte—and 90% of that maximum was then required while the total flux through reactions expressed below a threshold θ was minimised with weights θ − expression. Reactions were retained when their expression was at or above θ, when they lacked a gene rule, or when they carried flux in the GIMME solution. The primary threshold was the 25th percentile of reaction expression in each cell (4.6 nCPM in neurons, 6.3 nCPM in astrocytes); the 10th and 50th percentiles were used for sensitivity analysis.

Four curation steps encoded established neurochemistry that single-nucleus data capture poorly. Pyruvate carboxylase and glutamine synthetase were removed from the neuron, because both are astrocyte-restricted in the brain (Norenberg and Martinez-Hernandez 1979; Yu et al. 1983; Shank et al. 1985). The Na^+/K^+-ATPase (MAR05429) was restored in both cells: every one of its gene rules contains FXYD2, a regulatory subunit expressed mainly in the kidney and not required for pump activity (Geering 2008), so expression-based pruning removes the pump from every brain cell. The ATP-consuming vesicular glutamate transporter reaction (MAR05332; SLC17A6–8) was restored in the neuron to represent transmitter release. Finally, NAMPT and PRPP synthetase (NAD^+ salvage, both cells) and glutathione reductase with the oxidative pentose phosphate pathway (astrocyte) were retained at every threshold, because the most aggressive threshold prunes these steps, which every cell needs for NAD^+ salvage (Verdin 2015) or which are central to astrocytic glutathione recycling (Dringen et al. 2000); all were already present at the primary threshold, so only the 50th-percentile unit depends on this step.

Assembly of the neuron–astrocyte unit

The two context-specific networks were joined through a shared interstitial compartment that exchanges with blood. Every metabolite outside the extracellular compartment was made cell-specific, and a single set of exchange reactions connected the interstitial space with blood.

The assembled unit contained 20,029 reactions and 14,357 metabolites (9,179 neuronal and 9,196 astrocytic reactions).

Shared compartments create routes for free energy that real cells do not have, and the assembled unit initially passed ATP, sugar phosphates and other cofactors between the cells through generic transport entries. Transport across each plasma membrane was therefore restricted to 65 metabolites with documented transport in neurons or astrocytes (glucose, lactate, pyruvate, ketone bodies, acetate, amino acids including glutamate, glutamine and GABA, citrate, glutathione and its precursors, vitamins, essential fatty acids, inorganic ions, gases and water; full list in Online Resource 1, Table S1); 4,678 other transport reactions were closed. Release to blood was limited to CO_2, bicarbonate, water, protons, lactate, glutamine, alanine, ammonium, urea, sulfate, H_2S, taurine, urate and phosphate.

Ion and transmitter handling were then made explicit. Na^+ was allowed to leave either cell only through the Na^+/K^+-ATPase, and every Na^+-coupled transporter was restricted to its inward, gradient-driven direction. Astrocytic glutamate uptake was carried by the excitatory amino-acid transporter entry with its measured stoichiometry of three Na^+, one H^+ and one counter-transported K^+ per glutamate, shown for neuronal and glial transporters alike (Zerangue and Kavanaugh 1996; Levy et al. 1998); a duplicate one-Na^+ entry for the same genes was closed. Neuronal vesicular release was fixed at the glutamate–glutamine cycle rate Vcyc = 0.32 μmol g^{-1} min^{-1} measured in human cortex (Shen et al. 1999); astrocytic transporters were required to clear at least 90% of the released glutamate (Danbolt 2001), astrocytic glutamine synthetase to convert at least 90% of it to glutamine, and neuronal glutaminase to hydrolyse that glutamine. With these constraints the cost of clearing and recycling glutamate emerges from stoichiometry rather than being assigned.

Reactive oxygen species were represented by an electron-leak reaction that transfers electrons from ubiquinol to oxygen to form superoxide, coupled so that an assumed 0.2% of complex

IV oxygen flux is diverted to superoxide—of the order measured in isolated mitochondria (St-Pierre et al. 2002), whereas in vivo rates cannot be measured directly (Murphy 2009)—and varied from 0.1% to 1.0% in the sensitivity analyses. Cytosolic and mitochondrial catalase entries were closed, because catalase is peroxisomal and its activity in brain is low (Halliwell 2006); peroxisomal catalase was limited to 20% of the hydrogen peroxide formed, and glutathione peroxidases were required to clear the remainder. Glutathione reductase was constrained to its NADPH-dependent entries, and enzyme-free thiol–disulfide exchanges were prevented from regenerating reduced glutathione, so that peroxide clearance draws on NADPH supply. NAD^+ consumption by DNA-repair and NADase activity was coupled to superoxide formation (0.05 NAD^+ per leak event) and balanced by nicotinamide salvage through NAMPT (Verdin 2015).

Physiological calibration of the resting state

Blood supply ceilings were set from human physiology: glucose and oxygen at reserve multiples (below) of the unit's resting uptake, the glucose uptake being calibrated to the measured cerebral metabolic rate of glucose (CMRglc 0.31 μmol g^{-1} min^{-1}) (Madsen et al. 1995; Dienel 2019), so that the ceilings were 0.62 μmol glucose and 2.55 μmol O_2 g^{-1} min^{-1} (1.30 × the resting 1.96); the measured oxygen use ($CMRO_2$ about 1.5–1.6 μmol g^{-1} min^{-1} [Kety and Schmidt 1948]) was kept as a validation quantity; β-hydroxybutyrate 0.005, acetoacetate 0.003, acetate 0.003, glutamine 0.005 and ammonium 0.02 μmol g^{-1} min^{-1}; essential and conditionally essential amino acids 0.0005, vitamins and membrane precursors 0.0005, and essential fatty acids 0.0002 μmol g^{-1} min^{-1}; no net lactate uptake at rest. Glutamate exchange with blood was closed.

Resting ATP demand was divided among neuronal signalling (70%), neuronal housekeeping (20%) and astrocytic housekeeping (10%), following grey-matter energy budgets (Attwell and Laughlin 2001; Harris et al. 2012); the ATP spent on glutamate clearance, glutamine synthesis

and vesicular loading was not included in these shares, because it is generated by the network. The total resting demand T was the model's single calibrated parameter. It was chosen so that the solution meeting the demand with the least glucose consumed exactly the measured CMRglc; because the minimal glucose uptake is affine in T while supply is unconstrained, two evaluations fix it. Resting fluxes were then taken from the parsimonious solution (minimum total absolute flux) (Lewis et al. 2010a) with glucose uptake held at CMRglc. Quantities not used in calibration—oxygen use, the oxygen–glucose index, the astrocytic share of oxidation, neuronal tricarboxylic acid cycle flux, the Vcyc/TCA ratio and lactate exchange—were compared with independent human measurements (Kety and Schmidt 1948; Madsen et al. 1995; Shen et al. 1999; Gruetter et al. 2001; Lebon et al. 2002; Vaishnavi et al. 2010).

Reserves and the translation of behavioural stressors

Capacity limits were expressed as reserves over resting flux: mitochondrial capacity (complex IV and ATP synthase in each cell) R_ox = 1.25, the oxidative increase that grey matter recruits during strong stimulation (Lin et al. 2010); oxygen delivery R_O2 = 1.30, slightly above it; blood–brain glucose transport R_glc = 2.0, because maximal transport in the human brain (about 1.2 μmol g^{-1} min^{-1}) is several-fold resting use (Gruetter et al. 1992); and glutathione reductase and NAMPT capacity R_red = 2.0. These values are uncertain and were varied over wide ranges in the sensitivity analyses (R_ox 1.10–1.50; R_O2 1.10–1.60; R_glc 1.5–3.0; R_red 1.2–3.0; leak 0.1–1.0%). Because the arm with the smallest reserve binds first, the ordering of the reserves is itself an assumption, discussed below.

Five stressors were translated into constraints with the magnitudes of the pre-specified study protocol (the MSc research proposal on which this work is based; Table 1). The direction of each change is taken from the literature cited below; the magnitudes are protocol assumptions, which is why every one was varied continuously. Sustained cognitive load raised neuronal

signalling demand and, with it, Vcyc in the same proportion, as ^{13}C-MRS shows a one-to-one coupling between the cycle and neuronal glucose oxidation (Sibson et al. 1998). Sleep loss lowered the mitochondrial ceilings of both cells, representing the impaired mitochondrial homeostasis and energy restoration observed after sleep loss in animal studies (Dworak et al. 2010; Haynes et al. 2024). Circadian misalignment impairs systemic glucose tolerance (Scheer FAJL et al. 2009); its representation as a lower blood–brain glucose transport ceiling is a modelling assumption. Chronic psychosocial stress lowered the neuronal glucose uptake ceiling and raised housekeeping demand in both cells by the protocol amounts (McEwen 1998); in continuous sweeps a single intensity a raised maintenance by a and lowered glucose uptake by 2a/3, preserving the protocol's ratio (−20% and +30% at the high level). Chronic stress may also reduce mitochondrial capacity (Picard and McEwen 2018); that effect is captured by the sleep-loss arm and was not added here, which limits the estimated effect of stress. Reduced recovery lowered glutathione reductase and NAMPT capacity (Halliwell 2006; Verdin 2015). Low, moderate and high exposure applied all five together (Table 1), and continuous sweeps from 0 to 50% treated the three levels as anchors on a continuum. The combined path ran piecewise-linearly from rest through the moderate profile (scale 1) to the high profile (scale 2); the low profile lies at about 0.35–0.5 of the moderate one on this path. Because the unit represents a gram of engaged cortex rather than the whole brain, the cognitive-load levels refer to local, not global, increases in energy use (Raichle and Mintun 2006; Lin et al. 2010).

Readouts and the Brain Energetic Feasibility Index

Four readouts were computed for each condition. Neuronal ATP capacity C was the maximal neuronal ATP hydrolysis with astrocytic demand, the glutamate cycle and every coupling met. The energetic margin m = C/D_N relates capacity to the neuronal demand D_N of that condition; m < 1 means the demand cannot be met and the condition is infeasible. The ATP

production ratio is APR = C/C_0. The redox capacity ratio (RCR) is the headroom of glutathione recycling—reductase capacity minus the least reductase flux with which the demand and its superoxide load can be met—relative to rest. The feasibility volume ratio (FVR) is the geometric mean, over a panel of irreversible central reactions (hexokinase, phosphofructokinase, pyruvate kinase, pyruvate dehydrogenase, isocitrate and 2-oxoglutarate dehydrogenases, complexes I and IV, ATP synthase, glucose-6-phosphate dehydrogenase, glutathione peroxidase and reductase, in both cells), of the ratio of each flux range at the demand state to its resting range (Mahadevan and Schilling 2003); ranges bounded only by thermodynamically infeasible cycles (width $\geq$ 900) were excluded. Following the study protocol, the Brain Energetic Feasibility Index (BEFI) is the geometric mean of APR, FVR and RCR, set to zero when the demand cannot be met; the protocol's vulnerability boundary, BEFI 0.7 (30% of baseline feasibility lost), was used as a reference line.

Sensitivity, uncertainty, interaction and threshold analyses

Global sensitivity was estimated with Sobol indices (Sobol′ 2001; Saltelli 2002) over ten inputs—the five stressor intensities and the five reserve and leak parameters—using Saltelli sampling with N = 256 (3,072 evaluations) and first- and total-order indices for the margin, APR and RCR. Stressor ranges were cognitive load 0–50%, sleep loss 0–30%, circadian misalignment 0–20%, chronic stress 0–30% and reduced recovery 0–25%. Parameter uncertainty at each exposure level was propagated by Monte Carlo sampling of the five reserve and leak parameters (400 draws per level), giving the distribution of the margin and the probability that the demand can be met. As a control for circularity—the possibility that a stressor appears dominant only because the protocol assigns it a larger magnitude—the margin was recomputed after the same fractional perturbation (5, 10 and 20%) of each stressor. Pairwise interactions were mapped on 6 × 6 grids (0–50%) for all ten stressor pairs. Critical intensities, at which the margin reaches 1, were located by bisection (30 halvings)

between 0 and 95% for each stressor alone and between 0 and 2 on the combined path. Further tests varied the split of resting demand, imposed an enzyme-allocation constraint with random turnover numbers (Bar-Even et al. 2011; Sánchez et al. 2017) and clamped the direction of lactate exchange (Online Resource 1, Supplementary Methods).

Interventions

At moderate and high exposure, the margin was recomputed after removing each stressor in turn (sleep restored, circadian alignment, stress managed, recovery restored) or halving cognitive load, and after raising three nutritional supply ceilings: ketone bodies to nutritional-ketosis delivery (β-hydroxybutyrate 0.10, acetoacetate 0.03 μmol g^{-1} min^{-1}) (Owen et al. 1967; Hasselbalch et al. 1995), lactate to exercise-level delivery (0.10 μmol g^{-1} min^{-1}) (Quistorff et al. 2008; van Hall et al. 2009; van Hall 2010), and gut-derived acetate (0.03 μmol g^{-1} min^{-1}). Because these fuels can help only if glucose delivery limits, they were also tested in a glucose-limited state—no glucose-transport reserve (R_glc = 1.0) and 20% circadian misalignment—over a range of deliveries, at rest and at moderate exposure.

Day–night dynamics, regions and model quality

A seven-day simulation in 15-min steps followed astrocytic glycogen as a state variable through three sleep–wake schedules (Mahadevan et al. 2002; Öz et al. 2007); region-specific units were built from regional expression (Sjöstedt et al. 2020); and the unit was tested for mass and charge balance, energy-generating cycles (Fritzemeier et al. 2017; Lieven et al. 2020) and cycle-free solutions (Desouki et al. 2015), and the analyses were repeated across thresholds, Human-GEM v2.0.0, the HiGHS solver and Recon3D (Brunk et al. 2018) (Online Resource 1, Supplementary Methods).

Validation against human genetics

Each gene of the unit was deleted in both cells through its gene rules, and the resting margin was recomputed. A reference set of 24 genes (23 of them present in the unit) whose loss causes an inherited disorder of brain energy metabolism—GLUT1 deficiency, pyruvate dehydrogenase complex deficiency, pyruvate carboxylase deficiency, congenital glutamine deficiency, the mitochondrial aspartate–glutamate and glutamate carriers, and nuclear genes of complexes I to V and of the tricarboxylic acid cycle (De Vivo et al. 1991; Häberle et al. 2005; Molinari et al. 2005; Wibom et al. 2009; Marin-Valencia et al. 2010; Patel et al. 2012; Frazier et al. 2019)—was compared with all other genes of the unit by the fraction whose deletion lowered the resting margin by more than 1% and by the area under the receiver operating characteristic curve.

Statistics and reproducibility

The analysis is deterministic for a given input; stochastic components (Sobol and Monte Carlo sampling) used fixed seeds. Uncertainty is reported as 95% intervals of the Monte Carlo distributions and as bootstrap confidence intervals of Sobol indices. Differences between the disease-gene set and other genes were tested with Fisher's exact test and summarised by the area under the receiver operating characteristic curve. All code and computed tables are deposited (see Data Availability).

Results

A neuron–astrocyte unit that reproduces human brain energetics

Contextualisation retained 10,833 of 12,748 reactions in the neuron and 10,847 in the astrocyte; after the exchange reactions, which the unit holds once rather than per cell, and the curated reactions were accounted for, the assembled unit contained 20,029 reactions (9,179

neuronal and 9,196 astrocytic) and 14,357 metabolites. Before the transport and ion constraints were imposed, ATP-equivalents and phosphorylated intermediates passed from astrocyte to neuron through generic transport reactions, and glutamate clearance cost the astrocyte nothing. After transport was limited to metabolites with documented plasma-membrane carriers, Na^+ efflux to the Na^+/K^+-ATPase and glutamate uptake to the three-Na^+ transporter stoichiometry, each cell met its demand from its own mitochondria, and each glutamate cleared cost the astrocyte two ATP—one at the sodium pump and one at glutamine synthetase. The unit generated no ATP with all uptake closed, contained no energy-generating cycle, and its cycle-free solutions were identical to those reported (Online Resource 1, Table S11).

Calibration fixed the total resting ATP demand at 9.34 μmol g^{-1} min^{-1}, of which neuronal signalling took 6.54, neuronal housekeeping 1.87 and astrocytic housekeeping 0.93; the glutamate–glutamine cycle added 0.32 for vesicular loading, 0.29 for sodium pumping and 0.29 for glutamine synthesis (Fig. 1a, d). The quantities that were not calibrated were then compared with human measurements (Fig. 1b, c; Table 2). Astrocytes carried 15.7% of oxidative metabolism, against 14% measured with [2-^{13}C]acetate (Lebon et al. 2002); about 60% of astrocytic ATP use is the assigned housekeeping share and the remainder emerges from glutamate clearance. The astrocytic tricarboxylic acid (TCA) cycle rate was 0.10 μmol g^{-1} min^{-1}, inside the measured 0.14 ± 0.06, and the neuronal rate 0.56, so that the total TCA cycle rate was 0.66 against 0.77 ± 0.07 measured in occipital–parietal cortex (Shen et al. 1999). Because the unit is calibrated to whole-brain glucose use (0.31 μmol g^{-1} min^{-1}), whereas the cycle rate was measured in cortex where glucose oxidation is 0.39, the ratio of the glutamate–glutamine cycle to glucose oxidation is about 1.0 in the model against about 0.8 measured. Oxygen use was 1.96 μmol g^{-1} min^{-1}, about a quarter above the measured 1.5–1.6 (Kety and Schmidt 1948; Dienel 2019), and the oxygen–glucose index 6.3, above the

human range of about 4.1–5.5 (Fox et al. 1988; Madsen et al. 1995). Full oxidation of glucose alone gives an index of 6.0; the remainder, about 0.10 μmol O_2 g^{-1} min^{-1}, is the oxidation of the small supply of ketone bodies, acetate, glutamine and amino acids. The resting human brain instead metabolises about a tenth of its glucose non-oxidatively (Vaishnavi et al. 2010), so the model represents the most efficient use of the fuel it receives. No net lactate was released at rest. The unit could raise neuronal ATP production to 11.08 μmol g^{-1} min^{-1} against a demand of 8.40, an energetic margin of 1.32. With the same glucose and oxygen supply, a single-compartment Human-GEM produced at most 11.56 and Recon3D 11.80 μmol ATP g^{-1} min^{-1}, so the two reconstructions agree on the energetic yield of grey-matter fuel within 2%.

Graded behavioural exposure exhausts the margin

Each stressor of the study protocol was imposed alone and in combination (Fig. 2; Table 3). At the low level, all five together lowered the margin from 1.32 to 1.15 and the Brain Energetic Feasibility Index (BEFI) to 0.85 (Fig. 2c). At the moderate and high levels the combined profile could not be met: the margin fell to 0.89 and 0.56 and neuronal ATP capacity to 83% and 62% of rest. Across 400 draws of the five reserve and leak parameters, the resting demand was met in every draw (median margin 1.33, 95% interval 1.18–1.57), the low-exposure demand in 99.2% (1.17, 1.02–1.37), the moderate demand in 28.5% (0.94, 0.78–1.09) and the high demand in none (0.60, 0.48–0.71) (Fig. 2a; Table 4; Online Resource 1, Fig. S3).

Alone, sleep loss and cognitive load were the stressors that removed the margin within the protocol's range: at their high levels the margin fell to 0.93 and 0.94 (Fig. 2b). Chronic stress lowered it to 1.21 at its high level; circadian misalignment and reduced recovery left ATP capacity almost unchanged (margins 1.31 and 1.32), because they act on glucose transport and glutathione recycling, which retain reserve at rest. Reduced recovery nonetheless consumed

redox headroom—RCR fell to 0.54 at its high level—so that its effect appears in the index rather than in ATP capacity.

Thresholds

Continuous sweeps showed where each margin is exhausted (Fig. 3a, b; Table 5; Online Resource 1, Table S5). The critical intensity was 25.3% for loss of mitochondrial capacity, 39.1% for cognitive load, 50.0% for loss of glucose transport—the boundary set by the glucose-transport reserve itself (1 − 1/R_glc)—and 54.0% for loss of glutathione-recycling capacity; chronic stress did not exhaust the margin up to 95%. Recycling losses of up to 35% left the margin unchanged; beyond that, clearing the superoxide produced by oxidation began to draw on glucose that would otherwise yield ATP, and the margin fell steeply (1.28 at 40%, 1.19 at 45%, 1.09 at 50%) until it reached 1 at 54%. Along the combined path the margin fell almost linearly and reached 1 at 0.72 times the moderate profile, between the protocol's low and moderate levels. BEFI declined more steeply than ATP capacity, because pathway flexibility and redox headroom contract first (Fig. 3c): it crossed 0.7—the level at which 30% of baseline feasibility is lost, the vulnerability boundary pre-specified in the study protocol—at about 0.6 times the moderate profile, before the margin was exhausted.

Pathway flexibility contracts before capacity is lost

Flexibility of the irreversible central reactions contracted well before ATP capacity was lost (Fig. 4a). Under combined low exposure the flux ranges narrowed in both cells (FVR 0.79), and under moderate cognitive load or moderate sleep loss to 0.72 and 0.75; they collapsed when the demand could no longer be met. The ranges of neuronal complex IV and ATP synthase, the reactions that carry the binding constraint, narrowed most (to 0.53 and 0.58 of rest under combined low exposure and to 0.40 and 0.47 under moderate cognitive load).

Activation: oxidative support up to the mitochondrial ceiling, glycolytic beyond it

Raising neuronal signalling demand together with the glutamate–glutamine cycle reproduced the two regimes seen in human activation studies (Fig. 4b; Online Resource 1, Table S12). Up to a 21% increase in total ATP turnover, the increase was met entirely by oxidation: glucose and oxygen use rose by 22.9% and 21.7% respectively, with six molecules of oxygen per additional glucose and no lactate release, as in visual stimulation that raised ATP production by 12–17% with about 98% oxidative support (Lin et al. 2010). Beyond the mitochondrial ceiling, glucose uptake rose steeply (by 44% at a 24.5% increase in ATP turnover and by 93% at 27%), oxygen use peaked about 28% above rest, lactate was released (up to 0.42 μmol g^{-1} min^{-1}), and the incremental oxygen-to-glucose ratio fell from 6 to 1.65—the pattern of non-oxidative glucose consumption during focal activity, in which glucose uptake rose by 51% and oxygen use by 5% (Fox et al. 1988). The two observations, which have been read as contradictory, appear in the model as the two sides of one capacity limit.

Sleep loss at resting demand

With demand held at its resting value, losses of mitochondrial capacity of up to 20% left glucose and oxygen use unchanged (Fig. 4c; Online Resource 1, Table S13). Close to the threshold the remaining deficit was covered glycolytically—glucose uptake doubled and lactate was released—and beyond it the demand could no longer be met and the deliverable ATP fell by 7% at a 30% loss and by 35% at a 50% loss.

Mitochondrial capacity and demand, not the assigned magnitudes, set the ranking

Because the protocol assigns each stressor its own magnitude, a stressor could appear dominant only because it was given a large one. At equal perturbation the ranking was unchanged (Fig. 5b; Online Resource 1, Table S7): a 20% change removed 0.24 of margin through mitochondrial capacity, 0.18 through cognitive load, 0.08 through chronic stress, 0.01

through glucose transport and none through glutathione recycling. Global sensitivity analysis over all ten inputs together gave a consistent picture (Fig. 5a; Online Resource 1, Table S6). Cognitive load (total-order index 0.38), sleep loss (0.33) and the mitochondrial reserve (0.23)—the demand and the ceiling that must meet it—accounted for almost all of the variance in the margin; every other input had a total-order index below 0.04, and first-order indices were close to total-order indices, so the inputs acted mainly additively. Cognitive load probably ranked marginally above sleep loss here because its sampled range (0–50%) was wider than that of sleep loss (0–30%). Pairwise interactions were additive or sub-additive in seven of ten pairs (Online Resource 1, Fig. S4). The three pairs that combine circadian misalignment with sleep loss, cognitive load or reduced recovery were super-additive, by at most 0.02 of margin: once oxidation or redox recycling is limited, part of the deficit must be covered by glucose, which circadian misalignment then restricts. Cognitive load and sleep loss shared one ceiling, so that the feasible region was bounded by a nearly straight line from 39% load at no sleep loss to 25% sleep loss at no added load (Fig. 5c).

Dynamics: a small store refilled slowly

The seven-day simulation showed how the deficit develops when sleep is curtailed (Fig. 6). With 16 h awake and 8 h asleep at low exposure, the demand was met throughout, glycogen was never drawn on, and spare capacity during sleep filled the store from 3.5 to its maximum of 7.0 μmol glucosyl g^{-1}. With 19 h awake and 5 h asleep at the same exposure, the demand was met for two days; from day 3, as sleep debt lowered mitochondrial capacity, glycogen was mobilised and exhausted within about 3 h, after which part of the demand went unmet late in each waking period (3.5, 169 and 477 μmol ATP g^{-1} of unmet demand on days 3, 4 and 5; at most 10% of the instantaneous demand). At moderate exposure with the same schedule, glycogen was exhausted within the first hour and demand went unmet from the first day; the daily unmet demand grew from 1,857 to 3,301 μmol ATP g^{-1}, and the share of demand met

fell from 87% on day 1 to 76% on day 5 (worst instant 71%). In both curtailed schedules the first recovery night removed the deficit and two nights rebuilt glycogen to 6.3 of 7.0 μmol g^{-1}. The direction of these changes—depletion of brain glycogen with extended wakefulness and its restoration by recovery sleep—is that measured in the rat, where glycogen fell by about 40% after 12–24 h of sleep deprivation and recovered after 15 h of sleep (Kong et al. 2002).

Interventions: restore oxidation or lower demand; fuel does not help

At moderate exposure, restoring sleep returned the margin to 1.05, the only single measure that restored feasibility; halving cognitive load raised it to 0.98, managing stress to 0.93 and circadian alignment to 0.90, while restoring glutathione recycling had no effect on capacity (Fig. 7a). At high exposure the same order held (0.86, 0.67, 0.61 and 0.58 against 0.56). Raising the supply of ketone bodies to nutritional-ketosis delivery, of lactate to exercise-level delivery, or of gut-derived acetate did not change the margin at any level: the oxidation of any fuel is limited by the same mitochondria, and the extra fuel was not taken up. Alternative fuels mattered only when glucose delivery itself was made limiting, by removing the transport reserve and adding 20% circadian misalignment (Fig. 7b). The resting margin then fell to 0.77; ketone bodies at 0.10 μmol g^{-1} min^{-1} restored it to 1.07, lactate at 0.15 to 1.03, and fibre-derived acetate at 0.08 to 0.84 (Online Resource 1, Table S14), acetate being taken up almost entirely by the astrocyte, the property that makes [2-^{13}C]acetate an astrocytic marker in humans (Waniewski and Martin 1998; Lebon et al. 2002). Under moderate exposure on top of limited glucose delivery, no fuel raised the margin above 0.83, the mitochondrial ceiling.

The direction of lactate exchange is free

When the astrocyte's net lactate release was clamped at values from 0.3 μmol g^{-1} min^{-1} of uptake to 0.6 of release, the least total flux with which every demand could be met changed by less than 1.5%, at rest, under raised cognitive load and under sleep loss, with a shallow

minimum close to zero exchange (Online Resource 1, Table S15). The stoichiometry of grey matter therefore does not fix the direction of lactate exchange between the two cells, and none of the conclusions depends on it.

Robustness

The conclusions did not depend on the analytical choices tested (Online Resource 1, Table S8; Online Resource 1, Figs. S1–S3). Units built at the 10th and 50th percentile expression thresholds (22,421 and 16,181 reactions) gave resting margins of 1.34 and 1.34, low-exposure margins of 1.15 and 1.17, and moderate-exposure margins of 0.89 and 0.92; in both, the moderate profile could not be met and a 30% loss of mitochondrial capacity exhausted the margin (0.93 and 0.97). At the 50th percentile GIMME pruned NAMPT and PRPP synthetase in both cells and glutathione reductase and the oxidative pentose phosphate pathway in the astrocyte, the last two central to astrocytic glutathione recycling (Dringen et al. 2000) and the first two required by every cell for NAD^+ salvage (Verdin 2015); they were re-inserted at every threshold, and all were already present at the primary threshold, so only the 50th-percentile unit depends on this step. That unit calibrated to a lower resting demand (8.40 against 9.34 μmol ATP g^{-1} min^{-1}), and its high-exposure profile had no feasible solution at all. The same pipeline applied to Human-GEM v2.0.0 reproduced the primary results (margins 1.33, 1.16, 0.89 and 0.56 at rest and the three levels; astrocytic share of oxidation 15.0%). The HiGHS solver reproduced every GLPK capacity and margin to six decimal places. Varying the signalling share of resting demand from 60% to 80% changed no exposure-level margin by more than 0.01 and no single-stressor margin by more than 0.03, while the astrocytic share of oxidation ranged from 12.5% to 18.9%, bracketing the measured 14%. Under an enzyme-allocation constraint with 30 random sets of turnover numbers, rest and low exposure remained feasible in every set and moderate and high exposure infeasible in every set (Fig. 7c). Recon3D, under the same single-compartment set-up, lost ATP capacity under

mitochondrial and glucose-transport limits along closely parallel curves (within 0.05 of Human-GEM up to a 25% loss of mitochondrial capacity and within 0.07 at every point; Online Resource 1, Fig. S2).

Recovery of inherited brain-energy disorders

Deleting each of the 2,591 genes of the unit in both cells lowered the resting margin by more than 1% for 106 genes (Fig. 8a; Online Resource 1, Table S9). Seventeen of the 23 reference genes for inherited disorders of brain energy metabolism were among them, against 89 of the 2,568 other genes (odds ratio 79, Fisher's exact $p = 6 \times 10^{-20}$; area under the receiver operating characteristic curve 0.82; Fig. 8b). Deletion of the complex III subunit UQCRQ made the resting demand unmeetable, as did deletion of glutamine synthetase, which is unmeetable by construction because the glutamate–glutamine cycle is imposed; deletion of either of two ATP synthase subunits removed 94% of the margin, deletion of any of seven complex I subunits lowered it by 30%, and deletion of components of the pyruvate dehydrogenase complex, succinate dehydrogenase or fumarase lowered it by 10–12%. When isoforms not detected in the cell (nCPM < 1) were not allowed to substitute for the deleted gene—PDHA2, for example, is a testis-specific isoform of PDHA1—18 of 23 reference genes were recovered (odds ratio 97, $p = 1 \times 10^{-21}$, AUC 0.86). Because respiratory-chain genes are essential in most oxidative models, the strength of this association partly reflects the composition of the reference set. The genes that were not recovered are informative. GLUT1 (SLC2A1) deficiency was buffered by other glucose carriers and by the transport reserve, and the unit has no blood–brain barrier or endothelium, where GLUT1 deficiency acts; the mitochondrial aspartate–glutamate carrier (SLC25A12) and glutamate carrier (SLC25A22) have alternative shuttles in the reconstruction, and their deficiencies present as hypomyelination and neonatal epileptic encephalopathy (Molinari et al. 2005; Wibom et al. 2009), processes the model does not represent; succinyl-CoA ligase deficiency (SUCLA2)

was compensated by the GTP-forming isoform; and pyruvate carboxylase carried no flux at rest, so its loss is a deficit of anaplerosis under demand rather than of resting energy supply (Marin-Valencia et al. 2010).

Brain regions

Region-specific units built from bulk regional expression, with the astrocyte, glucose use and proportional reserves held constant by design, behaved almost identically (margins within 0.01 of one another at every level; Fig. 8c; Online Resource 1, Table S10); differences in enzyme content alone therefore do not reproduce the regional pattern of vulnerability after sleep deprivation (Thomas et al. 2000).

Discussion

The central result of this study is that, once the costs that bind neurons and astrocytes together are made explicit, the energetic margin of a model of human grey matter is set by mitochondrial oxidative capacity and by the demand it must meet. Sleep loss and sustained cognitive load each removed the margin on their own within the range of the study protocol; combined with circadian misalignment, chronic stress and reduced recovery, they did so at less than three-quarters of the moderate exposure profile. Circadian misalignment and reduced recovery acted on arms that retain reserve at rest—glucose transport and glutathione recycling—and became limiting only beyond the protocol's high level, and chronic stress, as represented here, did not become limiting within 0–95%. Neither fuel supply nor the direction of lactate exchange changed these conclusions, and the ranking held across expression thresholds, reconstruction releases, an independent reconstruction, a second solver, enzyme-capacity limits and wide uncertainty in every reserve.

The neuron–astrocyte unit reproduces key features of human brain energetics

A model of energetic limits is only as credible as its resting state. With a single calibrated quantity—the total resting ATP demand, fixed by the measured cerebral glucose use—the unit predicted an astrocytic share of oxidative metabolism of 15.7%, against 14% measured with [2-^{13}C]acetate in humans (Lebon et al. 2002), and an astrocytic tricarboxylic acid cycle rate within the measured interval. The share combines an assigned and an emergent component: the assigned astrocytic housekeeping (10% of resting demand) accounts for about 60% of astrocytic ATP use, and the remainder—two ATP for every glutamate cleared—emerges from the stoichiometry of the transporter and of glutamine synthetase (Pellerin and Magistretti 1994; Zerangue and Kavanaugh 1996; Levy et al. 1998). Across signalling shares of 60–80% the predicted share ranged from 12.5% to 18.9%, bracketing the measurement. Two further comparisons place the model relative to human data. Oxygen use was about a quarter above the measured value, and the oxygen–glucose index (6.3) above the human range of about 4.1–5.5 (Fox et al. 1988; Madsen et al. 1995), because the minimum-glucose solution oxidises every glucose molecule and the small supply of other fuels, whereas the resting human brain metabolises roughly a tenth of its glucose non-oxidatively (Vaishnavi et al. 2010). And because the unit is calibrated to whole-brain glucose use while the glutamate–glutamine cycle rate was measured in cortex, the ratio of the cycle to glucose oxidation is higher in the model (about 1.0) than in the measurement (about 0.8) (Shen et al. 1999). The model therefore describes the most efficient use of the fuel the brain receives, which makes its margins upper bounds and its thresholds conservative.

The response to activation is a sharper test, because two classic human studies appear to disagree. Lin and colleagues found that task-induced increases in ATP production of 12–17% were met almost entirely by oxidative metabolism (Lin et al. 2010), whereas Fox and colleagues found that glucose uptake rose ten times more than oxygen use (Fox et al. 1988).

The unit reproduced both, as two regimes of a single constraint. Up to an increase in ATP turnover of about one-fifth, glucose and oxygen use rose together in the ratio of complete oxidation, as in the first study; beyond the mitochondrial ceiling, further demand could be met only glycolytically, glucose uptake rose steeply, oxygen use stopped rising, and lactate was released, as in the second. The model thus places the boundary between the two observations at the mitochondrial reserve of the activated region, a quantitative prediction that combined ^{31}P and ^{13}C spectroscopy can test.

The model also recovered human genetics it was not built to reproduce. Deleting genes whose loss causes inherited disorders of brain energy metabolism lowered the resting margin far more often than deleting other metabolic genes (Fig. 8). The recovered genes are those of pyruvate oxidation, the respiratory chain, the tricarboxylic acid cycle and glutamine synthesis (Häberle et al. 2005; Patel et al. 2012; Frazier et al. 2019); glucose entry and anaplerosis were not compromised at rest, for reasons the model makes explicit—the absence of a blood–brain barrier in the unit, and an anaplerotic deficit that appears under demand rather than at rest (De Vivo et al. 1991; Marin-Valencia et al. 2010). Because respiratory-chain genes are essential in most oxidative models, the strength of the association partly reflects the composition of the reference set; its value is that the same structure that governs the stress responses also identifies the clinically indispensable steps.

Why mitochondrial capacity and demand, not fuel, set the margin

Three observations converge on this conclusion. First, at equal intensity, a reduction of mitochondrial capacity removed more margin than any other stressor, so the dominance of sleep loss is not an artefact of the magnitudes assigned by the study protocol (Fig. 5b). Second, global sensitivity analysis attributed most of the variance in the margin to cognitive load, sleep loss and the mitochondrial reserve—the demand and the ceiling that must meet it (Fig. 5a). Third, raising the supply of alternative oxidative substrates—fibre-derived acetate,

599 ketone bodies or lactate—did not restore the margin at any exposure level, because each must
600 still be oxidised by the same mitochondria (Fig. 7). These substrates mattered only when
601 glucose delivery itself was made limiting, the situation of hypoglycaemia or impaired
602 transport rather than of behavioural stress.
603 This conclusion is conditional in one important respect. Which arm binds first follows from
604 the relative reserves, and in every analysis the mitochondrial reserve was below the glucose-
605 transport and redox reserves. That ordering is supported by the evidence—maximal glucose
606 transport is several-fold resting use (Gruetter et al. 1992), whereas the oxidative response of
607 the cortex to strong stimulation is modest (Lin et al. 2010)—and by the agreement between
608 the model's activation response and human data, but it is an input to the model, not an output
609 of it. Within that ordering, the conclusion agrees with what is known about the cost of neural
610 signalling: mitochondria rather than glycolysis power presynaptic and postsynaptic
611 mechanisms (Hall et al. 2012), sleep loss impairs mitochondrial homeostasis (Haynes et al.
612 2024), and the brain has little room to expand oxidation on demand (Lin et al. 2010). It also
613 explains why glucose transport and the glutathione system, whose capacities exceed resting
614 need, become limiting only at extreme intensities or in combination. The implication for
615 intervention, if confirmed experimentally, is direct: measures that restore oxidative capacity
616 or lower demand restore the margin; measures that add fuel do not, unless glucose delivery is
617 the problem.

618 **Two responses at the limit, and what the data favour**

619 At the mitochondrial ceiling the network admits two responses. If neuronal demand is
620 defended, the deficit is covered by glycolysis: glucose uptake and lactate release rise steeply.
621 If demand is curtailed, glucose use falls and the work that cannot be paid for is not done. The
622 data are consistent with both, at different time scales. In rodents, extracellular lactate rises
623 across waking and falls during sleep (Naylor et al. 2012), and brain glycogen falls by about

40% after 12–24 h of sleep deprivation and recovers with sleep (Kong et al. 2002)—signs of a glycolytic defence of demand during extended wakefulness. In humans, after 24 h without sleep, cerebral glucose use falls globally, most strongly in the thalamus and prefrontal and parietal cortices, and alertness and performance fall with it (Thomas et al. 2000). In the model's terms, sustained sleep loss ends with the second response: the brain stops meeting the demand rather than paying for it, and the behavioural cost of sleep loss is the energetic cost made visible.

Dynamics: a small store, slowly refilled

The day–night simulation showed how this plays out over days. Under normal sleep at low exposure, the unit met its demand throughout and glycogen never had to be drawn on. Under sleep restriction at low exposure, demand exceeded capacity late in each extended day from day 3, glycogen covered the shortfall for about 3 h and was then exhausted; at moderate exposure, demand went unmet from the first day. One recovery night removed the deficit, and two rebuilt most of the store at an assumed refill rate about twice the bulk turnover measured in the human brain (Öz et al. 2007). Glycogen therefore buffers hours rather than days in this model, consistent with its measured content of a few micromoles per gram (Öz et al. 2007; Öz et al. 2015) and with its proposed role in the homeostatic drive to sleep (Benington and Heller 1995; Kong et al. 2002; Petit and Magistretti 2016).

Implications for metabolic nutrition

Seen through the lens of metabolic nutrition, the results separate substrate supply from substrate oxidation. Under behavioural stress the binding constraint in the model was the oxidation of substrate, not its supply: glucose delivery had reserve, and additional oxidative substrates—ketone bodies, lactate and acetate from the colonic fermentation of dietary fibre (Frost et al. 2014)—were not taken up, because the mitochondria that must oxidise them were

already at their ceiling. These substrates restored the margin only when glucose delivery was itself limiting, a situation closer to hypoglycaemia, impaired glucose transport or the insulin-resistant brain than to behavioural stress (Hasselbalch et al. 1995; Cunnane et al. 2020). Two hypotheses for nutrition practice follow, to be tested rather than applied. The first is that nutritional support of brain energy metabolism under chronic behavioural stress should be directed at the oxidative machinery and its micronutrient cofactors—thiamine for pyruvate dehydrogenase, riboflavin for the flavoproteins of the respiratory chain, niacin and nicotinamide for NAD^+ salvage, and sulfur amino acids for glutathione synthesis (Dringen et al. 2000; Verdin 2015)—rather than at a larger supply of substrate. The second is that ketogenic, exercise-lactate and fibre-rich strategies are most likely to benefit brain energy where glucose delivery is impaired. In both cases, the model places sleep and the structure of cognitive work ahead of diet as levers on the brain's energetic margin.

Relation to AI-intensive environments

The study models the behavioural profile rather than exposure to artificial intelligence itself, and it treats a given loss of sleep identically whatever its cause. Its claim is narrower and testable: the behavioural profile that AI-intensive environments are associated with—sustained cognitive engagement, shortened and mistimed sleep, persistent stress and reduced recovery (Chang et al. 2015; Hale and Guan 2015; Risko and Gilbert 2016; Gerlich 2025)—acts, in the model, through mitochondrial capacity and demand, and in combination exhausts the energetic margin well before any single stressor reaches its high level. The two links rest on different evidence. The link from behaviour to metabolism is tested quantitatively for cognitive load, against human activation data, and qualitatively for sleep loss, against human glucose-use data and rodent lactate and glycogen data; the representations of circadian misalignment, chronic stress and reduced recovery follow the literature, and their quantitative test is the next experimental step. The link from AI-intensive environments to the behaviours

673 rests on behavioural studies and is stated as such. What makes such environments distinctive
674 is not any one stressor but their co-occurrence, and the combined-exposure analysis is where
675 that co-occurrence matters: the stressors act on a shared ceiling, so that moderate amounts of
676 each can together remove a margin that none removes alone.

677 **Strengths, scope and tests**

678 Compared with earlier constraint-based brain models (Çakır et al. 2007; Lewis et al. 2010b;
679 Sertbaş et al. 2014), the study adds human single-nucleus contextualisation, explicit coupling
680 costs between the cells, validation against human measurements and genetics, and systematic
681 robustness tests.
682 The scope of the conclusions follows from the framework. Steady-state analysis describes
683 what the network permits, not how regulation chooses among permitted states; the two
684 responses at the limit are a case in point. Oxygen use and the oxygen–glucose index place the
685 model at the efficient end of brain metabolism, so the margins are upper bounds and the
686 thresholds conservative. The astrocytic share of oxidation depends on the assumed split of
687 resting demand. The stressor magnitudes come from the study protocol and were varied
688 continuously, and each stressor acts through the arm on which the evidence most consistently
689 places it: chronic stress through glucose uptake and maintenance, with its mitochondrial effect
690 (Picard and McEwen 2018) carried by the sleep-loss arm, and sleep loss through
691 mitochondrial capacity. Which arm binds first follows from the relative reserves, which were
692 ordered in every analysis. The dynamic analysis rests on rodent data for its direction and on
693 assumed rates of sleep-debt accumulation and glycogen refill. The unit is a gram of cortex
694 calibrated to whole-brain glucose use, has no blood–brain barrier, endothelium,
695 oligodendrocytes or microglia, and does not represent electrophysiology; the regional analysis
696 held demand and reserve constant by design; and single-nucleus data under-represent some
697 transcripts, which curation addressed for the best-documented cases only.

The model makes predictions that experiments can falsify. The critical mitochondrial reserve can be measured in human cortex with ^{31}P magnetisation transfer and calibrated functional imaging (Lei et al. 2003; Du et al. 2008); the transition from oxidative to glycolytic support of activation should occur at a lower stimulus intensity after sleep restriction; astrocytic oxidation measured with [2-^{13}C]acetate should rise with sustained cognitive load in proportion to the glutamate–glutamine cycle; and alternative fuels should not restore performance after sleep loss unless glucose delivery is impaired.

Conclusions

In a neuron–astrocyte model of human grey matter that reproduces key human ^{13}C-MRS and activation data and recovers the genetics of inherited brain-energy disorders, the energetic margin is set by mitochondrial oxidative capacity and the demand it must meet. Sleep loss and sustained cognitive load act directly on that margin and exhaust it on their own within the range studied; the five stressors associated with AI-intensive environments exhaust it together at less than three-quarters of the moderate profile. In the model, restoring sleep and reducing sustained load restore the margin, whereas additional fuel does not unless glucose delivery is limiting. In this model, brain vulnerability under chronic behavioural stress behaves as an energetic problem with a defined mechanism, quantitative thresholds and testable predictions.

References

Aiello LC, Wheeler P (1995) The Expensive-Tissue Hypothesis: The Brain and the Digestive System in Human and Primate Evolution. Curr Anthropol 36:199-221. https://doi.org/10.1086/204350

Attwell D, Laughlin SB (2001) An Energy Budget for Signaling in the Grey Matter of the Brain. J Cereb Blood Flow Metab 21:1133-1145. https://doi.org/10.1097/00004647-200110000-00001

722 Bar-Even A, Noor E, Savir Y et al (2011) The Moderately Efficient Enzyme: Evolutionary
723 and Physicochemical Trends Shaping Enzyme Parameters. Biochemistry 50:4402-4410.
724 https://doi.org/10.1021/bi2002289
725 Becker SA, Palsson BO (2008) Context-Specific Metabolic Networks Are Consistent with
726 Experiments. PLoS Comput Biol 4:e1000082.
727 https://doi.org/10.1371/journal.pcbi.1000082
728 Bélanger M, Allaman I, Magistretti PJ (2011) Brain Energy Metabolism: Focus on Astrocyte-
729 Neuron Metabolic Cooperation. Cell Metab 14:724-738.
730 https://doi.org/10.1016/j.cmet.2011.08.016
731 Benington JH, Heller HC (1995) Restoration of brain energy metabolism as the function of
732 sleep. Prog Neurobiol 45:347-360. https://doi.org/10.1016/0301-0082(94)00057-O
733 Brown AM, Ransom BR (2007) Astrocyte glycogen and brain energy metabolism. Glia
734 55:1263-1271. https://doi.org/10.1002/glia.20557
735 Brunk E, Sahoo S, Zielinski DC et al (2018) Recon3D enables a three-dimensional view of
736 gene variation in human metabolism. Nat Biotechnol 36:272-281.
737 https://doi.org/10.1038/nbt.4072
738 Çakır T, Alsan S, Saybaşılı H, Akın A, Ülgen KO (2007) Reconstruction and flux analysis of
739 coupling between metabolic pathways of astrocytes and neurons: application to cerebral
740 hypoxia. Theor Biol Med Model 4:48. https://doi.org/10.1186/1742-4682-4-48
741 Chang AM, Aeschbach D, Duffy JF, Czeisler CA (2015) Evening use of light-emitting
742 eReaders negatively affects sleep, circadian timing, and next-morning alertness. Proc Natl
743 Acad Sci USA 112:1232-1237. https://doi.org/10.1073/pnas.1418490112
744 Cunnane SC, Trushina E, Morland C et al (2020) Brain energy rescue: an emerging
745 therapeutic concept for neurodegenerative disorders of ageing. Nat Rev Drug Discov
746 19:609-633. https://doi.org/10.1038/s41573-020-0072-x

747 Danbolt NC (2001) Glutamate uptake. Prog Neurobiol 65:1-105.
748 https://doi.org/10.1016/S0301-0082(00)00067-8
749 De Vivo DC, Trifiletti RR, Jacobson RI, Ronen GM, Behmand RA, Harik SI (1991)
750 Defective Glucose Transport across the Blood-Brain Barrier as a Cause of Persistent
751 Hypoglycorrhachia, Seizures, and Developmental Delay. N Engl J Med 325:703-709.
752 https://doi.org/10.1056/NEJM199109053251006
753 Desouki AA, Jarre F, Gelius-Dietrich G, Lercher MJ (2015) CycleFreeFlux: efficient removal
754 of thermodynamically infeasible loops from flux distributions. Bioinformatics 31:2159-
755 2165. https://doi.org/10.1093/bioinformatics/btv096
756 Díaz-García CM, Mongeon R, Lahmann C, Koveal D, Zucker H, Yellen G (2017) Neuronal
757 Stimulation Triggers Neuronal Glycolysis and Not Lactate Uptake. Cell Metab 26:361-
758 374.e4. https://doi.org/10.1016/j.cmet.2017.06.021
759 Dienel GA (2019) Brain Glucose Metabolism: Integration of Energetics with Function.
760 Physiol Rev 99:949-1045. https://doi.org/10.1152/physrev.00062.2017
761 Dringen R, Gutterer JM, Hirrlinger J (2000) Glutathione metabolism in brain. Eur J Biochem
762 267:4912-4916. https://doi.org/10.1046/j.1432-1327.2000.01597.x
763 Du F, Zhu XH, Zhang Y et al (2008) Tightly coupled brain activity and cerebral ATP
764 metabolic rate. Proc Natl Acad Sci USA 105:6409-6414.
765 https://doi.org/10.1073/pnas.0710766105
766 Dworak M, McCarley RW, Kim T, Kalinchuk AV, Basheer R (2010) Sleep and Brain Energy
767 Levels: ATP Changes during Sleep. J Neurosci 30:9007-9016.
768 https://doi.org/10.1523/JNEUROSCI.1423-10.2010
769 Ebrahim A, Lerman JA, Palsson BO, Hyduke DR (2013) COBRApy: COnstraints-Based
770 Reconstruction and Analysis for Python. BMC Syst Biol 7:74.
771 https://doi.org/10.1186/1752-0509-7-74

772 Fox PT, Raichle ME, Mintun MA, Dence C (1988) Nonoxidative Glucose Consumption
773 During Focal Physiologic Neural Activity. Science 241:462-464.
774 https://doi.org/10.1126/science.3260686
775 Frazier AE, Thorburn DR, Compton AG (2019) Mitochondrial energy generation disorders:
776 genes, mechanisms, and clues to pathology. J Biol Chem 294:5386-5395.
777 https://doi.org/10.1074/jbc.R117.809194
778 Fritzemeier CJ, Hartleb D, Szappanos B, Papp B, Lercher MJ (2017) Erroneous energy-
779 generating cycles in published genome scale metabolic networks: Identification and
780 removal. PLoS Comput Biol 13:e1005494. https://doi.org/10.1371/journal.pcbi.1005494
781 Frost G, Sleeth ML, Sahuri-Arisoylu M et al (2014) The short-chain fatty acid acetate reduces
782 appetite via a central homeostatic mechanism. Nat Commun 5:3611.
783 https://doi.org/10.1038/ncomms4611
784 Geering K (2008) Functional roles of Na,K-ATPase subunits. Curr Opin Nephrol Hypertens
785 17:526-532. https://doi.org/10.1097/MNH.0b013e3283036cbf
786 Gerlich M (2025) AI Tools in Society: Impacts on Cognitive Offloading and the Future of
787 Critical Thinking. Societies 15:6. https://doi.org/10.3390/soc15010006
788 Gruetter R, Novotny EJ, Boulware SD et al (1992) Direct measurement of brain glucose
789 concentrations in humans by 13C NMR spectroscopy. Proc Natl Acad Sci USA 89:1109-
790 1112. https://doi.org/10.1073/pnas.89.3.1109
791 Gruetter R, Seaquist ER, Ugurbil K (2001) A mathematical model of compartmentalized
792 neurotransmitter metabolism in the human brain. Am J Physiol Endocrinol Metab
793 281:E100-E112. https://doi.org/10.1152/ajpendo.2001.281.1.E100
794 Häberle J, Görg B, Rutsch F et al (2005) Congenital Glutamine Deficiency with Glutamine
795 Synthetase Mutations. N Engl J Med 353:1926-1933.
796 https://doi.org/10.1056/NEJMoa050456

Hale L, Guan S (2015) Screen time and sleep among school-aged children and adolescents: A systematic literature review. Sleep Med Rev 21:50-58. https://doi.org/10.1016/j.smrv.2014.07.007

Hall CN, Klein-Flugge MC, Howarth C, Attwell D (2012) Oxidative Phosphorylation, Not Glycolysis, Powers Presynaptic and Postsynaptic Mechanisms Underlying Brain Information Processing. J Neurosci 32:8940-8951. https://doi.org/10.1523/JNEUROSCI.0026-12.2012

Halliwell B (2006) Oxidative stress and neurodegeneration: where are we now? J Neurochem 97:1634-1658. https://doi.org/10.1111/j.1471-4159.2006.03907.x

Harris JJ, Jolivet R, Attwell D (2012) Synaptic Energy Use and Supply. Neuron 75:762-777. https://doi.org/10.1016/j.neuron.2012.08.019

Hasselbalch SG, Knudsen GM, Jakobsen J, Hageman LP, Holm S, Paulson OB (1995) Blood-brain barrier permeability of glucose and ketone bodies during short-term starvation in humans. Am J Physiol Endocrinol Metab 268:E1161-E1166. https://doi.org/10.1152/ajpendo.1995.268.6.e1161

Haynes PR, Pyfrom ES, Li Y et al (2024) A neuron–glia lipid metabolic cycle couples daily sleep to mitochondrial homeostasis. Nat Neurosci 27:666-678. https://doi.org/10.1038/s41593-023-01568-1

Herculano-Houzel S (2011) Scaling of Brain Metabolism with a Fixed Energy Budget per Neuron: Implications for Neuronal Activity, Plasticity and Evolution. PLoS One 6:e17514. https://doi.org/10.1371/journal.pone.0017514

Herman J, Usher W (2017) SALib: An open-source Python library for Sensitivity Analysis. J Open Source Softw 2:97. https://doi.org/10.21105/joss.00097

Hertz L, Peng L, Dienel GA (2007) Energy Metabolism in Astrocytes: High Rate of Oxidative Metabolism and Spatiotemporal Dependence on Glycolysis/Glycogenolysis. J Cereb Blood Flow Metab 27:219-249. https://doi.org/10.1038/sj.jcbfm.9600343

Huangfu Q, Hall JAJ (2018) Parallelizing the dual revised simplex method. Math Program Comput 10:119-142. https://doi.org/10.1007/s12532-017-0130-5

Jamadar SD, Behler A, Deery H, Breakspear M (2025) The metabolic costs of cognition. Trends Cogn Sci 29:541-555. https://doi.org/10.1016/j.tics.2024.11.010

Jensen K, Cardoso JGR, Sonnenschein N (2017) Optlang: An algebraic modeling language for mathematical optimization. J Open Source Softw 2:139. https://doi.org/10.21105/joss.00139

Karlsson M, Zhang C, Méar L et al (2021) A single–cell type transcriptomics map of human tissues. Sci Adv 7:eabh2169. https://doi.org/10.1126/sciadv.abh2169

Kety SS, Schmidt CF (1948) The nitrous oxide method for the quantitative determination of cerebral blood flow in man: theory, procedure and normal values. J Clin Invest 27:476-483. https://doi.org/10.1172/JCI101994

Kong J, Shepel PN, Holden CP, Mackiewicz M, Pack AI, Geiger JD (2002) Brain Glycogen Decreases with Increased Periods of Wakefulness: Implications for Homeostatic Drive to Sleep. J Neurosci 22:5581-5587. https://doi.org/10.1523/JNEUROSCI.22-13-05581.2002

Lebon V, Petersen KF, Cline GW et al (2002) Astroglial contribution to brain energy metabolism in humans revealed by 13C nuclear magnetic resonance spectroscopy: elucidation of the dominant pathway for neurotransmitter glutamate repletion and measurement of astrocytic oxidative metabolism. J Neurosci 22:1523-1531. https://doi.org/10.1523/JNEUROSCI.22-05-01523.2002

Lei H, Ugurbil K, Chen W (2003) Measurement of unidirectional P i to ATP flux in human visual cortex at 7 T by using in vivo 31P magnetic resonance spectroscopy. Proc Natl Acad Sci USA 100:14409-14414. https://doi.org/10.1073/pnas.2332656100

Levy LM, Warr O, Attwell D (1998) Stoichiometry of the Glial Glutamate Transporter GLT-1 Expressed Inducibly in a Chinese Hamster Ovary Cell Line Selected for Low Endogenous Na+-Dependent Glutamate Uptake. J Neurosci 18:9620-9628. https://doi.org/10.1523/JNEUROSCI.18-23-09620.1998

Lewis NE, Hixson KK, Conrad TM et al (2010a) Omic data from evolved E. coli are consistent with computed optimal growth from genome-scale models. Mol Syst Biol 6:390. https://doi.org/10.1038/msb.2010.47

Lewis NE, Schramm G, Bordbar A et al (2010b) Large-scale in silico modeling of metabolic interactions between cell types in the human brain. Nat Biotechnol 28:1279-1285. https://doi.org/10.1038/nbt.1711

Lieven C, Beber ME, Olivier BG et al (2020) MEMOTE for standardized genome-scale metabolic model testing. Nat Biotechnol 38:272-276. https://doi.org/10.1038/s41587-020-0446-y

Lin AL, Fox PT, Hardies J, Duong TQ, Gao JH (2010) Nonlinear coupling between cerebral blood flow, oxygen consumption, and ATP production in human visual cortex. Proc Natl Acad Sci USA 107:8446-8451. https://doi.org/10.1073/pnas.0909711107

Mächler P, Wyss MT, Elsayed M et al (2016) In Vivo Evidence for a Lactate Gradient from Astrocytes to Neurons. Cell Metab 23:94-102. https://doi.org/10.1016/j.cmet.2015.10.010

Madsen PL, Hasselbalch SG, Hagemann LP et al (1995) Persistent Resetting of the Cerebral Oxygen/Glucose Uptake Ratio by Brain Activation: Evidence Obtained with the Kety–Schmidt Technique. J Cereb Blood Flow Metab 15:485-491. https://doi.org/10.1038/jcbfm.1995.60

868 Magistretti PJ, Allaman I (2015) A Cellular Perspective on Brain Energy Metabolism and
869 Functional Imaging. Neuron 86:883-901. https://doi.org/10.1016/j.neuron.2015.03.035
870 Mahadevan R, Schilling CH (2003) The effects of alternate optimal solutions in constraint-
871 based genome-scale metabolic models. Metab Eng 5:264-276.
872 https://doi.org/10.1016/j.ymben.2003.09.002
873 Mahadevan R, Edwards JS, Doyle FJ (2002) Dynamic Flux Balance Analysis of Diauxic
874 Growth in Escherichia coli. Biophys J 83:1331-1340. https://doi.org/10.1016/S0006-
875 3495(02)73903-9
876 Marin-Valencia I, Roe CR, Pascual JM (2010) Pyruvate carboxylase deficiency: Mechanisms,
877 mimics and anaplerosis. Mol Genet Metab 101:9-17.
878 https://doi.org/10.1016/j.ymgme.2010.05.004
879 McEwen BS (1998) Protective and Damaging Effects of Stress Mediators. N Engl J Med
880 338:171-179. https://doi.org/10.1056/NEJM199801153380307
881 Molinari F, Raas-Rothschild A, Rio M et al (2005) Impaired Mitochondrial Glutamate
882 Transport in Autosomal Recessive Neonatal Myoclonic Epilepsy. Am J Hum Genet
883 76:334-339. https://doi.org/10.1086/427564
884 Murphy MP (2009) How mitochondria produce reactive oxygen species. Biochem J 417:1-13.
885 https://doi.org/10.1042/BJ20081386
886 Naylor E, Aillon DV, Barrett BS et al (2012) Lactate as a Biomarker for Sleep. Sleep
887 35:1209-1222. https://doi.org/10.5665/sleep.2072
888 Norenberg MD, Martinez-Hernandez A (1979) Fine structural localization of glutamine
889 synthetase in astrocytes of rat brain. Brain Res 161:303-310.
890 https://doi.org/10.1016/0006-8993(79)90071-4

Owen OE, Morgan AP, Kemp HG, Sullivan JM, Herrera MG, Cahill GF (1967) Brain metabolism during fasting. J Clin Invest 46:1589-1595. https://doi.org/10.1172/JCI105650

Öz G, Seaquist ER, Kumar A et al (2007) Human brain glycogen content and metabolism: implications on its role in brain energy metabolism. Am J Physiol Endocrinol Metab 292:E946-E951. https://doi.org/10.1152/ajpendo.00424.2006

Öz G, DiNuzzo M, Kumar A, Moheet A, Seaquist ER (2015) Revisiting Glycogen Content in the Human Brain. Neurochem Res 40:2473-2481. https://doi.org/10.1007/s11064-015-1664-4

Patel KP, O'Brien TW, Subramony SH, Shuster J, Stacpoole PW (2012) The spectrum of pyruvate dehydrogenase complex deficiency: Clinical, biochemical and genetic features in 371 patients. Mol Genet Metab 106:385-394. https://doi.org/10.1016/j.ymgme.2012.03.017

Pellerin L, Magistretti PJ (1994) Glutamate uptake into astrocytes stimulates aerobic glycolysis: a mechanism coupling neuronal activity to glucose utilization. Proc Natl Acad Sci USA 91:10625-10629. https://doi.org/10.1073/pnas.91.22.10625

Petit JM, Magistretti PJ (2016) Regulation of neuron–astrocyte metabolic coupling across the sleep–wake cycle. Neuroscience 323:135-156. https://doi.org/10.1016/j.neuroscience.2015.12.007

Picard M, McEwen BS (2018) Psychological Stress and Mitochondria: A Systematic Review. Psychosom Med 80:141-153. https://doi.org/10.1097/PSY.0000000000000545

Quistorff B, Secher NH, Van Lieshout JJ (2008) Lactate fuels the human brain during exercise. FASEB J 22:3443-3449. https://doi.org/10.1096/fj.08-106104

Rae CD, Baur JA, Borges K et al (2024) Brain energy metabolism: A roadmap for future research. J Neurochem 168:910-954. https://doi.org/10.1111/jnc.16032

916 Raichle ME, Mintun MA (2006) Brain work and brain imaging. Annu Rev Neurosci 29:449-
917 476. https://doi.org/10.1146/annurev.neuro.29.051605.112819
918 Risko EF, Gilbert SJ (2016) Cognitive Offloading. Trends Cogn Sci 20:676-688.
919 https://doi.org/10.1016/j.tics.2016.07.002
920 Robinson JL, Kocabaş P, Wang H et al (2020) An atlas of human metabolism. Sci Signal
921 13:eaaz1482. https://doi.org/10.1126/scisignal.aaz1482
922 Saltelli A (2002) Making best use of model evaluations to compute sensitivity indices.
923 Comput Phys Commun 145:280-297. https://doi.org/10.1016/S0010-4655(02)00280-1
924 Sánchez BJ, Zhang C, Nilsson A, Lahtvee P, Kerkhoven EJ, Nielsen J (2017) Improving the
925 phenotype predictions of a yeast genome-scale metabolic model by incorporating
926 enzymatic constraints. Mol Syst Biol 13:935. https://doi.org/10.15252/msb.20167411
927 Scheer FAJL, Hilton MF, Mantzoros CS, Shea SA (2009) Adverse metabolic and
928 cardiovascular consequences of circadian misalignment. Proc Natl Acad Sci USA
929 106:4453-4458. https://doi.org/10.1073/pnas.0808180106
930 Sertbaş M, Ülgen K, Çakır T (2014) Systematic analysis of transcription-level effects of
931 neurodegenerative diseases on human brain metabolism by a newly reconstructed brain-
932 specific metabolic network. FEBS Open Bio 4:542-553.
933 https://doi.org/10.1016/j.fob.2014.05.006
934 Shank RP, Bennett GS, Freytag SO, Campbell GL (1985) Pyruvate carboxylase: an astrocyte-
935 specific enzyme implicated in the replenishment of amino acid neurotransmitter pools.
936 Brain Res 329:364-367. https://doi.org/10.1016/0006-8993(85)90552-9
937 Shen J, Petersen KF, Behar KL et al (1999) Determination of the rate of the
938 glutamate/glutamine cycle in the human brain by in vivo 13C NMR. Proc Natl Acad Sci
939 USA 96:8235-8240. https://doi.org/10.1073/pnas.96.14.8235

Sibson NR, Dhankhar A, Mason GF, Rothman DL, Behar KL, Shulman RG (1998) Stoichiometric coupling of brain glucose metabolism and glutamatergic neuronal activity. Proc Natl Acad Sci USA 95:316-321. https://doi.org/10.1073/pnas.95.1.316

Siletti K, Hodge R, Mossi Albiach A et al (2023) Transcriptomic diversity of cell types across the adult human brain. Science 382:eadd7046. https://doi.org/10.1126/science.add7046

Sjöstedt E, Zhong W, Fagerberg L et al (2020) An atlas of the protein-coding genes in the human, pig, and mouse brain. Science 367:eaay5947. https://doi.org/10.1126/science.aay5947

Sobol′ IM (2001) Global sensitivity indices for nonlinear mathematical models and their Monte Carlo estimates. Math Comput Simul 55:271-280. https://doi.org/10.1016/S0378-4754(00)00270-6

Spiegel K, Leproult R, Van Cauter E (1999) Impact of sleep debt on metabolic and endocrine function. Lancet 354:1435-1439. https://doi.org/10.1016/S0140-6736(99)01376-8

St-Pierre J, Buckingham JA, Roebuck SJ, Brand MD (2002) Topology of Superoxide Production from Different Sites in the Mitochondrial Electron Transport Chain. J Biol Chem 277:44784-44790. https://doi.org/10.1074/jbc.M207217200

Thomas M, Sing H, Belenky G et al (2000) Neural basis of alertness and cognitive performance impairments during sleepiness. I. Effects of 24 h of sleep deprivation on waking human regional brain activity. J Sleep Res 9:335-352. https://doi.org/10.1046/j.1365-2869.2000.00225.x

Uhlén M, Fagerberg L, Hallström BM et al (2015) Tissue-based map of the human proteome. Science 347:1260419. https://doi.org/10.1126/science.1260419

Vaccaro A, Kaplan Dor Y, Nambara K et al (2020) Sleep Loss Can Cause Death through Accumulation of Reactive Oxygen Species in the Gut. Cell 181:1307-1328.e15. https://doi.org/10.1016/j.cell.2020.04.049

965 Vaishnavi SN, Vlassenko AG, Rundle MM, Snyder AZ, Mintun MA, Raichle ME (2010)
966 Regional aerobic glycolysis in the human brain. Proc Natl Acad Sci USA 107:17757-
967 17762. https://doi.org/10.1073/pnas.1010459107
968 van Hall G (2010) Lactate kinetics in human tissues at rest and during exercise. Acta Physiol
969 199:499-508. https://doi.org/10.1111/j.1748-1716.2010.02122.x
970 van Hall G, Strømstad M, Rasmussen P et al (2009) Blood Lactate is an Important Energy
971 Source for the Human Brain. J Cereb Blood Flow Metab 29:1121-1129.
972 https://doi.org/10.1038/jcbfm.2009.35
973 Verdin E (2015) NAD+ in aging, metabolism, and neurodegeneration. Science 350:1208-
974 1213. https://doi.org/10.1126/science.aac4854
975 Waniewski RA, Martin DL (1998) Preferential Utilization of Acetate by Astrocytes Is
976 Attributable to Transport. J Neurosci 18:5225-5233.
977 https://doi.org/10.1523/JNEUROSCI.18-14-05225.1998
978 Wibom R, Lasorsa FM, Töhönen V et al (2009) AGC1 Deficiency Associated with Global
979 Cerebral Hypomyelination. N Engl J Med 361:489-495.
980 https://doi.org/10.1056/NEJMoa0900591
981 Wu JC, Gillin JC, Buchsbaum MS et al (1991) The effect of sleep deprivation on cerebral
982 glucose metabolic rate in normal humans assessed with positron emission tomography.
983 Sleep 14:155-162. https://doi.org/10.1093/sleep/14.2.155
984 Yellen G (2018) Fueling thought: Management of glycolysis and oxidative phosphorylation in
985 neuronal metabolism. J Cell Biol 217:2235-2246. https://doi.org/10.1083/jcb.201803152
986 Yu ACH, Drejer J, Hertz L, Schousboe A (1983) Pyruvate Carboxylase Activity in Primary
987 Cultures of Astrocytes and Neurons. J Neurochem 41:1484-1487.
988 https://doi.org/10.1111/j.1471-4159.1983.tb00849.x

989 Zerangue N, Kavanaugh MP (1996) Flux coupling in a neuronal glutamate transporter. Nature
990 383:634-637. https://doi.org/10.1038/383634a0
991

Statements and Declarations

Funding

This research received no specific grant from any funding agency in the public, commercial or not-for-profit sectors.

Competing Interests

Christina Charles and Jofrey Raymond are affiliated with BioNutra Company Limited, which provided the computing infrastructure on which the analyses were run. The company had no role in the design of the study, the interpretation of the results or the decision to publish. The other authors declare no competing interests.

Author Contributions

Shangwe Leonard Kigoda: conceptualisation, methodology, formal analysis, investigation, visualisation, writing of the original draft. Christina Charles: software, data curation, validation, writing (review and editing). Musa Chacha: supervision, writing (review and editing). Jofrey Raymond: conceptualisation, methodology, supervision, validation, writing (review and editing). All authors read and approved the final manuscript.

Ethics Approval

This study used only public reconstructions and public, de-identified, aggregate expression data. No human participants or animals were involved, and ethics approval was therefore not required.

Consent to Participate

Not applicable; no human participants were involved.

Consent to Publish

Not applicable; the article contains no individual person's data.

Data Availability

Human-GEM v2.1.1 is available from the SysBioChalmers repository (https://github.com/SysBioChalmers/Human-GEM), Recon3D from the BiGG database (http://bigg.ucsd.edu/models/Recon3D), and the single-cell type and brain-region expression tables from the Human Protein Atlas (https://www.proteinatlas.org/about/download). The computed result tables and constraint definitions are deposited at Zenodo (https://doi.org/10.5281/zenodo.23757900) under a CC BY 4.0 licence.

Code Availability

All analysis code (Python; COBRApy-based model construction, constraint definitions, simulations and figure scripts) is deposited at Zenodo (https://doi.org/10.5281/zenodo.23757900) under the MIT licence.

Tables

Table 1 Translation of the five behavioural stressors into constraints (study protocol magnitudes, relative to rest)

Stressor	Metabolic translation	Constraint changed	Low	Moderate	High
Sustained cognitive load	Higher neuronal ATP turnover and glutamate cycling	Neuronal signalling demand and Vcyc raised	+10%	+25%	+50%
Sleep loss	Reduced mitochondrial efficiency	Complex IV and ATP synthase ceilings (both cells) lowered	−5%	−15%	−30%
Circadian misalignment	Reduced glucose-transport efficiency	Blood–brain glucose transport ceiling lowered	−5%	−10%	−20%
Chronic psychosocial	Impaired glucose uptake; higher	Neuronal glucose-uptake	−3% / +5%	−10% / +15%	−20% / +30%

stress	maintenance	ceiling lowered / housekeeping demand raised			
Reduced recovery	Weaker redox recycling	Glutathione reductase and NAMPT ceilings lowered	−5%	−15%	−25%

1030

1031 **Table 2** Resting state of the unit against human measurements

Quantity (µmol g^{-1} min^{-1} unless stated)	**Model**	**Human measurement**	**Method**	**Status**
Cerebral glucose use (CMRglc)	0.31	0.31	Arteriovenous difference; FDG-PET	Calibrated
Glutamate–glutamine cycle (Vcyc)	0.32	0.32 ± 0.05	^{13}C-MRS, human cortex	Imposed
Astrocytic share of O_2 use	15.7%	14%	[2-^{13}C]acetate MRS	Predicted
Astrocytic TCA cycle	0.10	0.14 ± 0.06	[2-^{13}C]acetate MRS	Predicted
Total TCA cycle	0.66	0.77 ± 0.07	[1-^{13}C]glucose MRS	Predicted
Cerebral O_2 use ($CMRO_2$)	1.96	1.5–1.6	Kety–Schmidt (arteriovenous)	Predicted
O_2 : glucose	6.3	4.1–5.5	PET; arteriovenous difference	Predicted
Na^+/K^+-ATPase flux for glutamate clearance	0.29	1 ATP per glutamate (3 Na^+)	Transporter stoichiometry	Emergent

1032

1033 **Table 3** Energetic readouts under graded exposure (fluxes in µmol g^{-1} min^{-1})

Exposure	**Level**	**Neuronal ATP capacity**	**Neuronal demand**	**Margin**	**APR**	**FVR**	**RCR**	**BEFI**
Rest	—	11.08	8.40	1.32	1.00	1.00	1.00	1.00
All five combined	Low	10.50	9.15	1.15	0.95	0.79	0.81	0.85
All five combined	Moderate	9.16	10.32	0.89	0.83	0 (infeasible)	0	0.00
All five combined	High	6.86	12.23	0.56	0.62	0 (infeasible)	0	0.00
Cognitive load	Low	11.05	9.06	1.22	1.00	0.92	0.93	0.95
Cognitive load	Moderate	11.00	10.04	1.10	0.99	0.72	0.81	0.84
Cognitive load	High	10.92	11.67	0.94	0.99	0 (infeasible)	0	0.00
Sleep loss	Low	10.57	8.40	1.26	0.95	0.93	1.00	0.96
Sleep loss	Moderate	9.56	8.40	1.14	0.86	0.75	1.00	0.86
Sleep loss	High	7.84	8.40	0.93	0.71	0 (infeasible)	0	0.00
Circadian misalignment	Low	11.08	8.40	1.32	1.00	0.99	0.99	0.99
Circadian misalignment	Moderate	11.08	8.40	1.32	1.00	0.97	0.99	0.99
Circadian misalignment	High	10.99	8.40	1.31	0.99	0.93	0.98	0.97
Chronic stress	Low	11.05	8.50	1.30	1.00	0.98	0.99	0.99
Chronic stress	Moderate	10.96	8.68	1.26	0.99	0.95	0.96	0.96
Chronic	High	10.83	8.96	1.21	0.98	0.89	0.92	0.93

stress								
Reduced recovery	Low	11.08	8.40	1.32	1.00	0.99	0.91	0.97
Reduced recovery	Moderate	11.08	8.40	1.32	1.00	0.98	0.72	0.89
Reduced recovery	High	11.08	8.40	1.32	1.00	0.97	0.54	0.80

Table 4 Margin across 400 draws of the reserve and leak parameters

Exposure	**Median margin**	**95% interval**	**Draws meeting demand**
Rest	1.33	1.18–1.57	100.0%
Low	1.17	1.02–1.37	99.2%
Moderate	0.94	0.78–1.09	28.5%
High	0.60	0.48–0.71	0.0%

Table 5 Critical intensities at which the energetic margin reaches 1

Stressor	**Critical intensity (margin = 1)**
Cognitive load	39.1%
Sleep loss	25.3%
Circadian misalignment	50.0%
Chronic stress	not reached (≤95%)
Reduced recovery	54.0%
All five combined	0.72 × moderate profile

Figure legends

Fig. 1 The resting neuron–astrocyte unit and its agreement with human measurements. **a** Resting fluxes of the two-cell unit (μmol g^{-1} min^{-1}): blood supply, neuronal and astrocytic ATP demand, the glutamate–glutamine cycle and the oxidative fluxes of each cell. **b** Rates predicted by the model (filled) or set from data (open) against human measurements (grey bars; CMRglc and $CMRO_2$ from arteriovenous and PET studies, cycle and tricarboxylic acid cycle rates from ^{13}C magnetic resonance spectroscopy). **c** Astrocytic share of oxygen use and the oxygen-to-glucose ratio against human ranges. **d** Resting ATP budget; the three components of the glutamate–glutamine cycle—vesicular loading, Na^+ pumping and glutamine synthesis—emerge from stoichiometry.

Fig. 2 Graded exposure to the five behavioural stressors. a Energetic margin (neuronal ATP capacity divided by neuronal demand) at rest and under combined low, moderate and high exposure. Boxes and whiskers summarise 400 draws of the five reserve and leak parameters (50% and 95% intervals); open circles mark the primary parameter set; numbers give the share of draws in which demand is met. **b** Margin under each stressor alone at the protocol's low, moderate and high levels (light to dark). **c** Components of the Brain Energetic Feasibility Index—ATP production ratio, feasibility volume ratio and redox capacity ratio—and the index itself; the index is zero when demand cannot be met.

Fig. 3 Thresholds. a Margin against the intensity of each stressor alone; dots mark critical intensities at which the margin reaches 1. **b** Margin along the combined exposure path (moderate profile = 1, high = 2); the margin is exhausted at 0.72 times the moderate profile. **c** Components of the Brain Energetic Feasibility Index along the combined path; flexibility and redox headroom contract before ATP capacity, and the index crosses the vulnerability boundary of 0.7 before the margin is exhausted.

Fig. 4 Mechanism: flexibility, activation and sleep loss. a Flux range of irreversible central reactions in neurons (N) and astrocytes (A) relative to rest under each exposure (blank where the demand cannot be met). **b** Raising neuronal signalling demand together with the glutamate–glutamine cycle: glucose and oxygen use rise together while the mitochondrial reserve lasts (shaded band: human activation, ATP production +12–17%, about 98% oxidative); beyond it, glucose use and lactate release rise while oxygen use stops rising. **c** Loss of mitochondrial capacity at resting demand: margin, glucose use if the demand is defended glycolytically, and the share of demand that can be met.

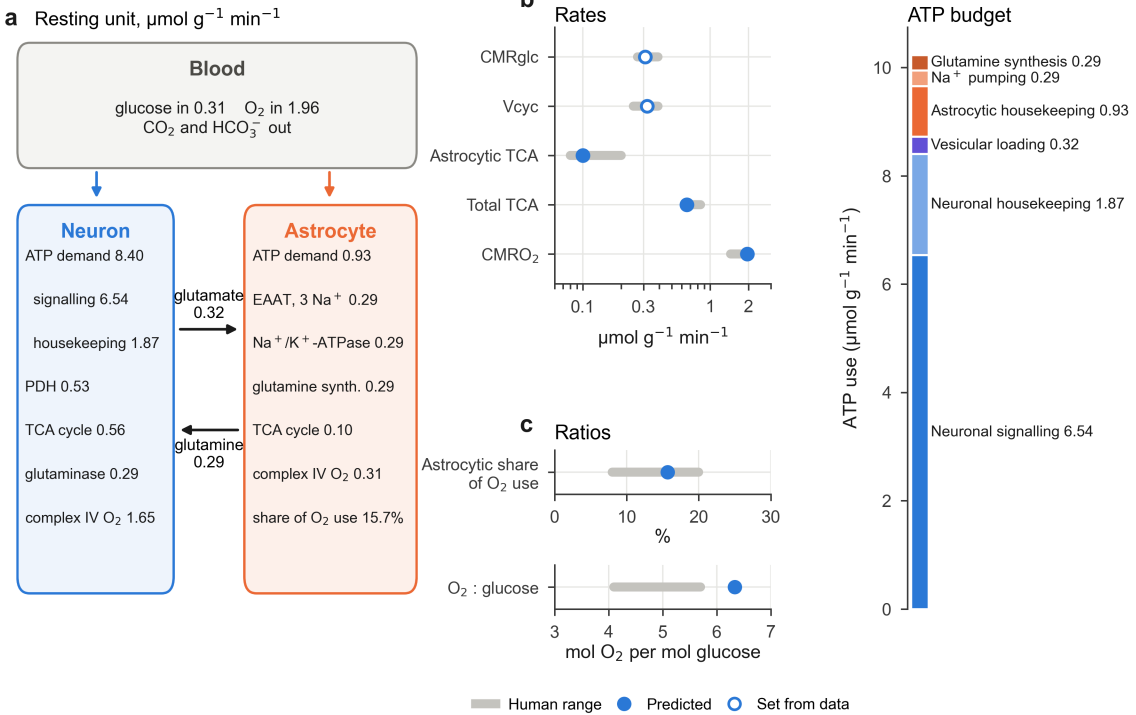
Fig. 5 Sensitivity and interaction. a Total-order Sobol indices (bars, with 95% bootstrap intervals) and first-order indices (white ticks) for the energetic margin over five stressors and five reserve and leak parameters (3,072 evaluations). **b** Loss of margin after the same 5, 10 and 20% perturbation of each stressor (light to dark), a control for the magnitudes assigned in the protocol. **c** Margin over cognitive load and sleep loss together; the black line marks margin = 1.

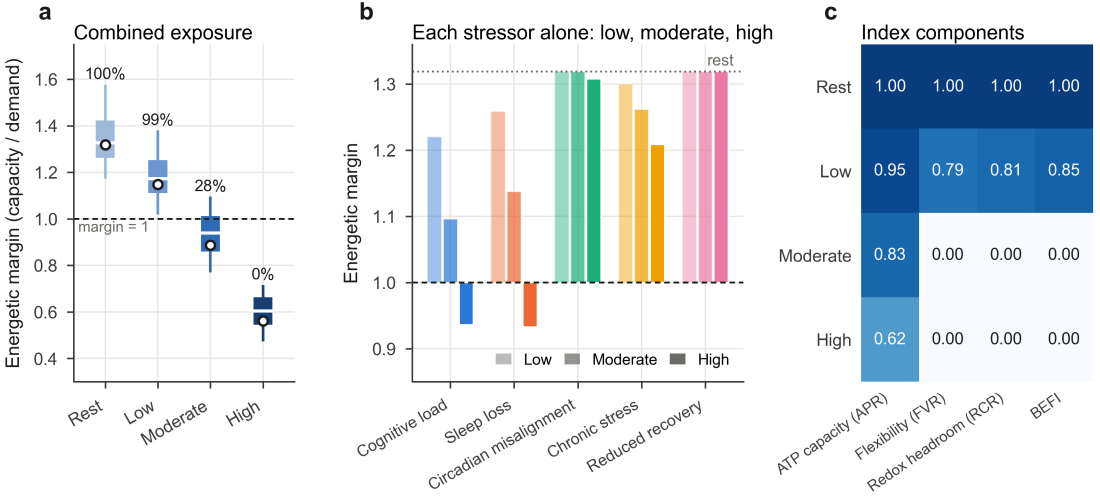
Fig. 6 Day–night dynamics with astrocytic glycogen. Seven-day simulation in 15-min steps for three schedules, with two recovery nights from day 5 (shaded). **a** Astrocytic glycogen. **b** Share of neuronal demand met.

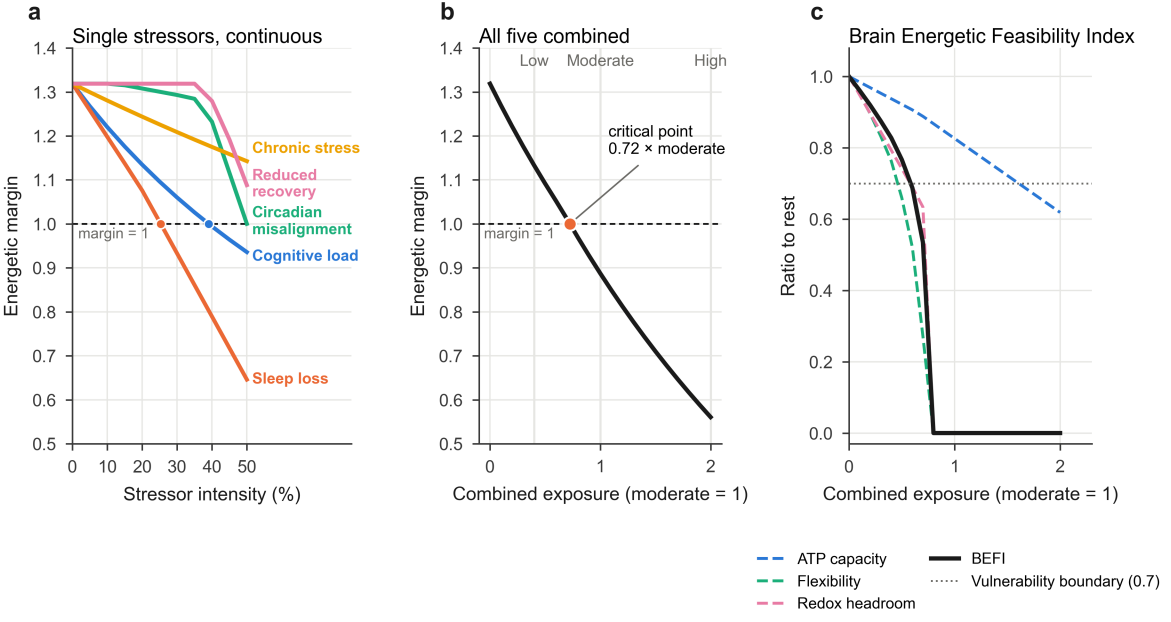
Fig. 7 Interventions, alternative fuels and enzyme capacity. a Margin regained by each intervention at moderate and high exposure. **b** Margin against the delivery of ketone bodies, lactate or gut-derived acetate when glucose delivery limits (no transport reserve, circadian misalignment 20%), at rest (solid) and moderate exposure (dashed). **c** Margin under an enzyme-allocation constraint with 30 random sets of turnover numbers drawn from the measured distribution (dots) and without it (bars).

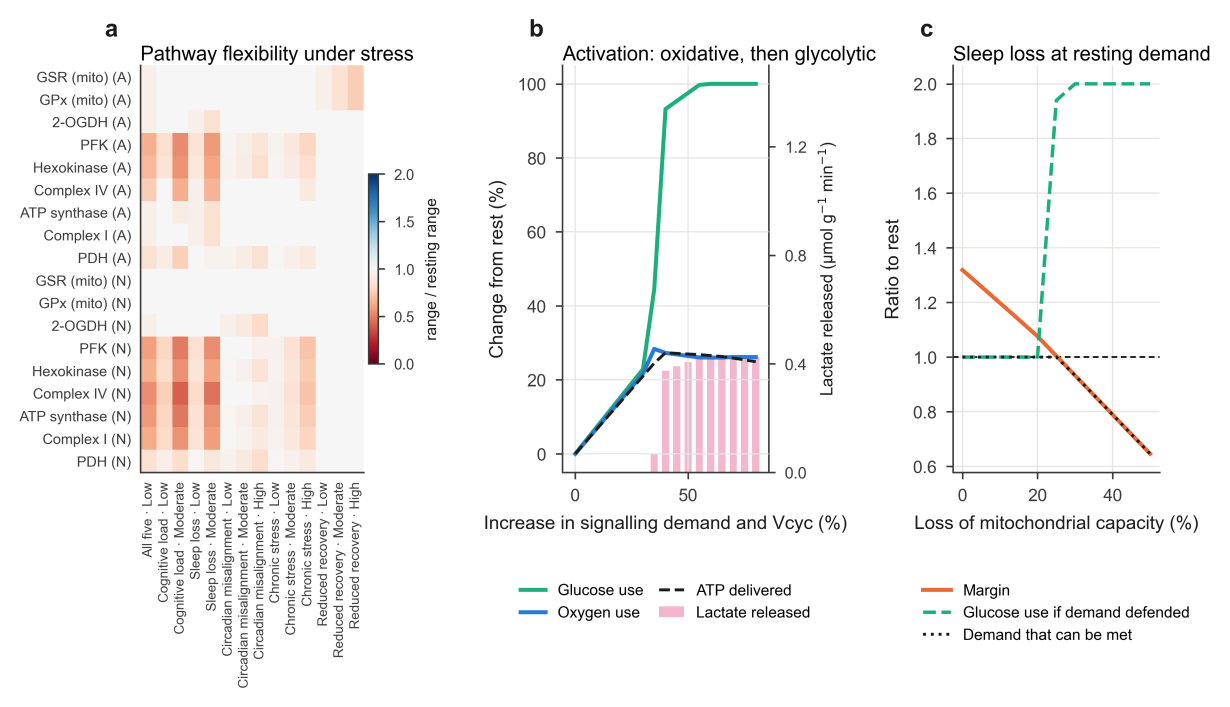
Fig. 8 Validation against human genetics and regional vulnerability. a Resting margin after deletion of each gene of the unit, relative to the intact unit; red marks genes whose loss

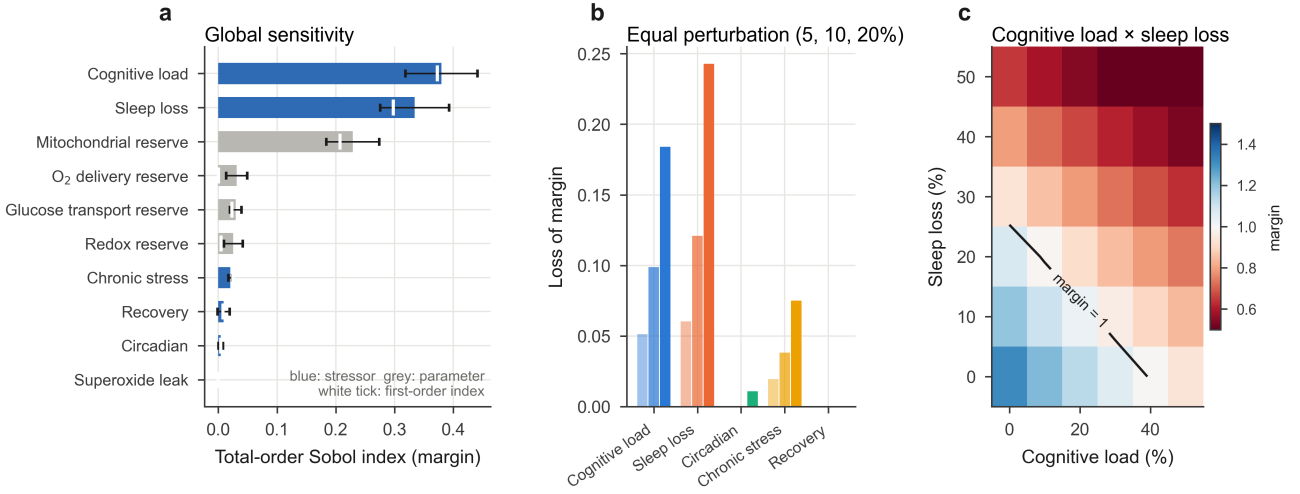
causes an inherited disorder of brain energy metabolism. **b** Receiver operating characteristic for the recovery of those genes, with all isoforms (solid) and with isoforms not detected in the cell excluded from compensation (dashed). **c** Margin of region-specific units at rest, at low exposure, with 30% loss of mitochondrial capacity and at moderate exposure.

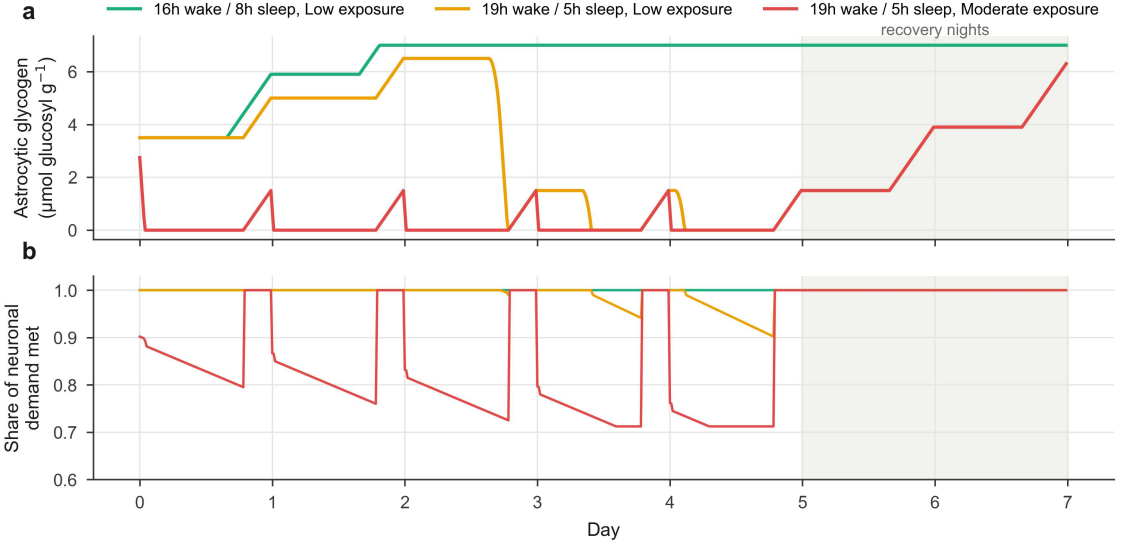

a
Resting unit, μmol g−1 min−1
Blood
glucose in 0.31 O2 in 1.96
CO2 and HCO3− out
Neuron
ATP demand 8.40
signalling 6.54
housekeeping 1.87
PDH 0.53
TCA cycle 0.56
glutaminase 0.29
complex IV O2 1.65
Astrocyte
ATP demand 0.93
EAAT, 3 Na+ 0.29
Na+/K+-ATPase 0.29
glutamine synth. 0.29
TCA cycle 0.10
complex IV O2 0.31
share of O2 use 15.7%
glutamate 0.32
glutamine 0.29
b
Rates
CMRglc
Vcyc
Astrocytic TCA
Total TCA
CMRO2
0.1
0.3
1
2
μmol g−1 min−1
c
Ratios
Astrocytic share of O2 use
0
10
20
30
%
O2 : glucose
3
4
5
6
7
mol O2 per mol glucose
d
ATP budget
ATP use (μmol g−1 min−1)
0
2
4
6
8
10
Glutamine synthesis 0.29
Na+ pumping 0.29
Astrocytic housekeeping 0.93
Vesicular loading 0.32
Neuronal housekeeping 1.87
Neuronal signalling 6.54
Human range
Predicted
Set from data

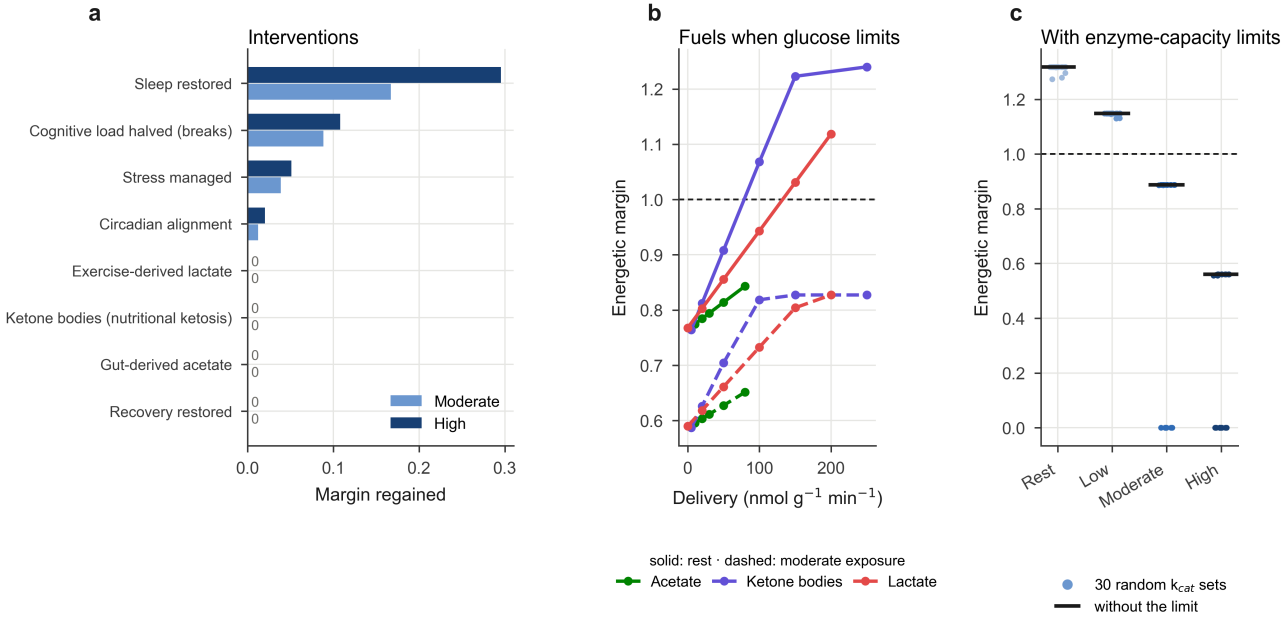

a
Combined exposure
Energetic margin (capacity / demand)
1.6
1.4
1.2
1.0
0.8
0.6
0.4
100%
99%
28%
0%
margin = 1
Rest
Low
Moderate
High
b
Each stressor alone: low, moderate, high
Energetic margin
1.3
1.2
1.1
1.0
0.9
rest
Low
Moderate
High
Cognitive load
Sleep loss
Circadian misalignment
Chronic stress
Reduced recovery
c
Index components
Rest
Low
Moderate
High
1.00
1.00
1.00
1.00
0.95
0.79
0.81
0.85
0.83
0.00
0.00
0.00
0.62
0.00
0.00
0.00
ATP capacity (APR)
Flexibility (FVR)
Redox headroom (RCR)
BEFI

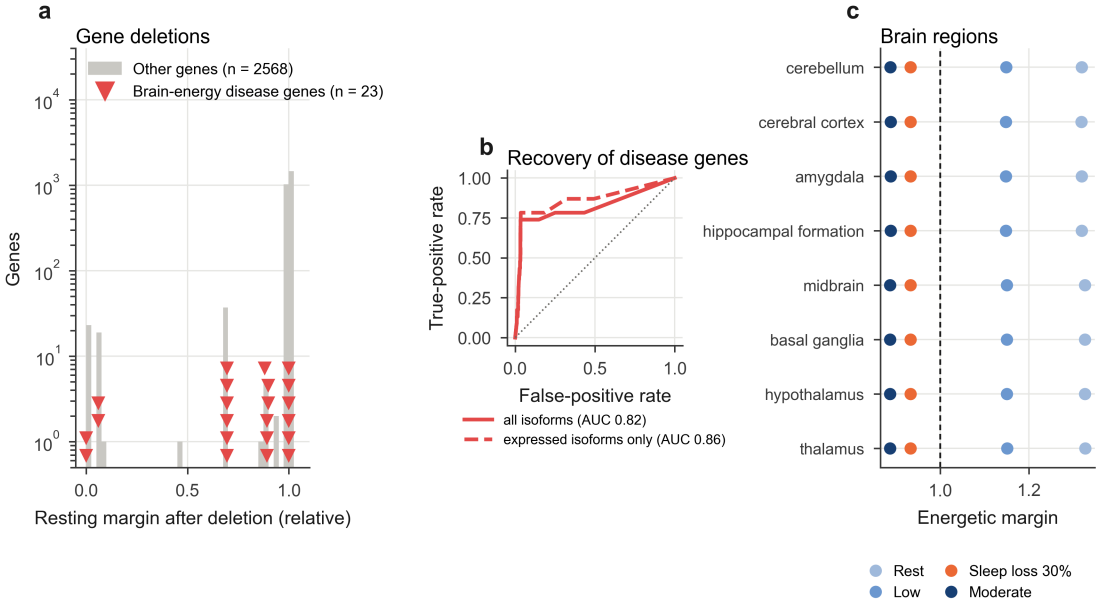

a
Single stressors, continuous
Energetic margin
Stressor intensity (%)
margin = 1
Chronic stress
Reduced recovery
Circadian misalignment
Cognitive load
Sleep loss
b
All five combined
Low
Moderate
High
critical point
0.72 × moderate
Energetic margin
Combined exposure (moderate = 1)
margin = 1
c
Brain Energetic Feasibility Index
Ratio to rest
Combined exposure (moderate = 1)
ATP capacity
Flexibility
Redox headroom
BEFI
Vulnerability boundary (0.7)


a
Pathway flexibility under stress
GSR (mito) (A)
GPx (mito) (A)
2-OGDH (A)
PFK (A)
Hexokinase (A)
Complex IV (A)
ATP synthase (A)
Complex I (A)
PDH (A)
GSR (mito) (N)
GPx (mito) (N)
2-OGDH (N)
PFK (N)
Hexokinase (N)
Complex IV (N)
ATP synthase (N)
Complex I (N)
PDH (N)
All five · Low
Cognitive load · Low
Cognitive load · Moderate
Sleep loss · Low
Sleep loss · Moderate
Circadian misalignment · Low
Circadian misalignment · Moderate
Circadian misalignment · High
Chronic stress · Low
Chronic stress · Moderate
Chronic stress · High
Reduced recovery · Low
Reduced recovery · Moderate
Reduced recovery · High
2.0
1.5
1.0
0.5
0.0
range / resting range
b
Activation: oxidative, then glycolytic
Change from rest (%)
Lactate released (µmol g⁻¹ min⁻¹)
Increase in signalling demand and Vcyc (%)
Glucose use
Oxygen use
ATP delivered
Lactate released
c
Sleep loss at resting demand
Ratio to rest
Loss of mitochondrial capacity (%)
Margin
Glucose use if demand defended
Demand that can be met


a
Global sensitivity
Cognitive load
Sleep loss
Mitochondrial reserve
O2 delivery reserve
Glucose transport reserve
Redox reserve
Chronic stress
Recovery
Circadian
Superoxide leak
blue: stressor grey: parameter
white tick: first-order index
0.0
0.1
0.2
0.3
0.4
Total-order Sobol index (margin)
b
Equal perturbation (5, 10, 20%)
Loss of margin
0.25
0.20
0.15
0.10
0.05
0.00
Cognitive load
Sleep loss
Circadian
Chronic stress
Recovery
c
Cognitive load × sleep loss
Sleep loss (%)
50
40
30
20
10
0
margin = 1
1.4
1.2
1.0
0.8
0.6
margin
0
20
40
Cognitive load (%)


a
16h wake / 8h sleep, Low exposure
19h wake / 5h sleep, Low exposure
19h wake / 5h sleep, Moderate exposure
recovery nights
Astrocytic glycogen (µmol glucosyl g^{-1})
0
2
4
6
b
Share of neuronal demand met
0.6
0.7
0.8
0.9
1.0
0
1
2
3
4
5
6
7
Day


a
Interventions
Sleep restored
Cognitive load halved (breaks)
Stress managed
Circadian alignment
Exercise-derived lactate
Ketone bodies (nutritional ketosis)
Gut-derived acetate
Recovery restored
0
0
0
0
0
0
Moderate
High
0.0
0.1
0.2
0.3
Margin regained
b
Fuels when glucose limits
Energetic margin
1.2
1.1
1.0
0.9
0.8
0.7
0.6
0
100
200
Delivery (nmol g^{-1} min^{-1})
solid: rest · dashed: moderate exposure
Acetate
Ketone bodies
Lactate
c
With enzyme-capacity limits
Energetic margin
1.2
1.0
0.8
0.6
0.4
0.2
0.0
Rest
Low
Moderate
High
30 random k_{cat} sets
without the limit


a
Gene deletions
Other genes (n = 2568)
Brain-energy disease genes (n = 23)
Genes
10^4
10^3
10^2
10^1
10^0
0.0
0.5
1.0
Resting margin after deletion (relative)
b
Recovery of disease genes
True-positive rate
1.00
0.75
0.50
0.25
0.00
0.0
0.5
1.0
False-positive rate
all isoforms (AUC 0.82)
expressed isoforms only (AUC 0.86)
c
Brain regions
cerebellum
cerebral cortex
amygdala
hippocampal formation
midbrain
basal ganglia
hypothalamus
thalamus
1.0
1.2
Energetic margin
Rest
Low
Sleep loss 30%
Moderate